

MULTIFREQUENCY RADIO OBSERVATIONS OF CYGNUS A: SPECTRAL AGING IN POWERFUL RADIO GALAXIES

C. L. CARILLI,¹ R. A. PERLEY,¹ J. W. DREHER,² AND J. P. LEAHY^{1,3}

Received 1990 January 31; accepted 1991 June 26

ABSTRACT

We present a detailed analysis of the radio spectrum across the lobes of Cygnus A. These observations provide the first critical test of synchrotron spectral aging theory. The results are in good agreement with the jet model for powerful radio galaxies, involving particle acceleration at the hot spots and outflow into the radio lobes, with subsequent energy loss due to synchrotron radiation. The hot spot spectra are well represented by a spectral aging model involving continuous injection of relativistic particles. Both hot spots have spectral break frequencies around 10 GHz. We find an injection index of -0.5 for both hot spots, consistent with diffusive shock acceleration at a strong, nonrelativistic shock in a Newtonian fluid. The low-frequency hot spot emission spectrum falls below the injected power law. This effect is isolated to the hot spots, and is best explained by a low-energy cutoff in the particle distribution, as predicted by Bell in his original work on diffusive shock acceleration. We find that expansion losses may be significant going from the hot spots to the lobes, but that beyond a few arcseconds from the hot spots the dominant energy loss mechanism is synchrotron radiation. The break frequency distribution across each lobe shows a clear trend of decreasing break frequency with distance from the hot spot. The lowest break frequency in the source is 750 MHz, which implies a source age of 6 Myr in minimum-energy magnetic fields. The separation velocity assuming minimum-energy fields is $0.06c$ ($H_0 = 75 \text{ km s}^{-1} \text{ Mpc}^{-1}$). This is much larger than the source advance speed required for ram-pressure confinement of the heads of the lobes, assuming a minimum-energy configuration for the particles and fields. A self-consistent model is possible in which the fields are a factor of 3 below minimum-energy values. This results in a source advance speed approximately equal to the separation velocity, $\approx 0.01c$, and a source age of 30 Myr.

The lobe spectra fall off more steeply than allowed by the continuous injection model at high frequency, but less steeply than exponential. The lobe spectra are well represented by a spectral model involving “one-shot” injection and subsequent energy loss through synchrotron radiation, without continuous isotropization of the pitch-angle distribution. At $1''.5$ resolution, we find break frequencies much greater than 10 GHz beyond $2''$ from the hot spots. This is inconsistent with a simple hot spot model involving particle injection at a single point and radiative losses in an axisymmetric outflow from this point, and suggests spatially distributed particle acceleration in the vicinity of the hot spots and/or highly asymmetric outflow. We also find that the injection index across the lobes is -0.7 . Such a value is difficult to reconcile with the observed hot spot injection indices of -0.5 . The cause for this injection index discrepancy remains a mystery.

Subject headings: galaxies: individual (Cygnus A) — galaxies: jets — radiation mechanisms — radio sources: galaxies

1. INTRODUCTION

The basic model of the generation and evolution of luminous extragalactic radio sources was developed by Blandford & Rees (1974) and by Scheuer (1974). They postulated a cold, highly collimated, high-velocity flow formed within or near the active galaxy nucleus. This flow propagates without significant dissipation to the ends of the radio-emitting lobes, where it shocks and terminates, converting much of its bulk kinetic energy into relativistic electrons and magnetic fields.

This basic model explains in a simple way the components of highly luminous extragalactic radio sources: The unresolved core corresponds to the nucleus of the galaxy, from which the collimated flow emerges; the radio-emitting jets trace the path of the flow as it passes through the evacuated lobes; the bright hot spots mark the strong shock where the cold flow is shocked

and heated upon impinging the external medium; and the radio-emitting lobes contain the outflow from the shock. The momentum of the jet moves the hot spots forward into the surrounding medium, and the lobes grow in size and luminosity with what might be called the “waste products” of the process.

Since the seminal works of Blandford & Rees and Scheuer, a very large body of observational evidence has strongly supported this basic model. This work includes detailed studies of the nucleus, the jets, and the hot spots of powerful radio galaxies. Reviews of these subjects can be found in Zensus & Pearson (1990), Bridle & Perley (1984), and Röser & Meisenheimer (1989). Work on radio lobes includes a detailed study of the large-scale morphology of radio “bridges” (Leahy & Williams 1984) and the discovery of small-scale “filamentary” structures in radio lobes (Perley, Dreher, & Cowan 1984; Fomalont et al. 1989; Hines, Owen, & Eilek 1990).

It is well known that the radio spectra of powerful radio galaxies (Class II sources; Fanaroff & Riley 1974) steepen going from the hot spots at the ends of the lobes back toward the core radio source. This spectral morphology has been

¹ National Radio Astronomy Observatory, P.O. Box O, Socorro, NM 87801.

² MS 238-22, NASA-Ames Research Center, Moffett Field, CA 94035.

³ Postal address: Nuffield Radio Astronomy Laboratories, Jodrell Bank, Macclesfield, Cheshire SK11 9DL, England, UK.

explained as a radiative aging effect of the relativistic electrons. Such spectral steepening supports the idea that the electrons at the center of the source are "older" than those closer to the hot spots. The inference is that the source is expanding in time, in agreement with the basic source model. The connection between radio spectrum and age allows a study of the growth and evolution of the lobes by careful measurement of the spectrum throughout the length and width of the source.

Considerable effort has been expended to measure spectral variations across powerful radio galaxies, and to relate these measurements to source dynamics (Burch 1979; Alexander 1985, 1987; Alexander & Leahy 1987; Myers & Spangler 1985; Stephens 1987). These studies all support the basic jet model for radio galaxies. Typical velocities for the radiating fluid in radio lobes measured by synchrotron aging analyses range from 0.02 to 0.2 times the speed of light (assuming minimum-energy fields). For Cygnus A, the synchrotron aging study of Winter et al. (1980), using radio observations at three frequencies, yielded a source of age 6 Myr, and a flow velocity in the radio lobes of 0.03c. Alexander et al. (1984) performed a similar analysis of Cygnus A, at higher spatial resolution, and derived a somewhat higher flow velocity in the Cygnus A radio lobes of 0.07c.

The principal difficulty with the study of synchrotron aging in radio galaxies is that the high-frequency steepening expected from synchrotron radiation losses occurs over a very broad range in frequency (see § 2). Hence, proper analysis of the radio spectrum of extended extragalactic radio sources requires sensitive observations to be made over a broad range in frequency. A further difficulty is that the spectrum varies with position in the source. Hence, observations at all frequencies must be spatially resolved and of matched spatial resolution. Virtually all previous observational work on this problem has been limited by lack of spatial resolution, frequency coverage, or sensitivity. Indeed, although the theoretical spectral models of the synchrotron aging process have been widely used in the study of powerful radio galaxies, no observations to date have been adequate to either confirm or reject any of the hypothetical models.

As part of an overall study of Cygnus A, we have for some years been collecting data at all VLA observing bands in all configurations (Carilli et al. 1989b; Carilli, Dreher, & Perley 1989a; Carilli, Perley, & Dreher 1988; Dreher, Carilli, & Perley 1987a, b; Perley et al. 1984). In this paper, we present our extensive observations and theoretical analysis of the radio spectrum of Cygnus A. Cygnus A is clearly the best source on which to conduct a multifrequency radio spectral analysis, owing to its proximity (redshift = 0.057; Spinrad & Stauffer 1982) and high surface brightness over a broad range in frequency. These multifrequency, high dynamic range, spatially resolved radio observations of Cygnus A represent the most extensive radio spectral study of a powerful radio galaxy to date, and allow critical tests of particle acceleration theory, synchrotron aging theory, and dynamical models for radio sources.

2. SYNCHROTRON AGING

2.1. Basic Theory

The generally power-law spectra and high linear polarization of the extended radio emission from radio galaxies and quasars provide strong evidence that the radiation is due to synchrotron emission by relativistic electrons spiraling in weak

magnetic fields. The theory of synchrotron emission and radiative aging of relativistic electrons in cosmic radio sources is well developed. Reviews can be found in articles by Kardashev (1962) and Scheuer & Williams (1968), and in textbooks by Pacholczyk (1970, 1977). We briefly review the basic theory, and give some details concerning the specific physical processes considered in this paper.

The total power, P , emitted by an electron of energy, $\gamma m_e c^2$, is given by $P = K_1 \gamma^2 B^2 \sin^2 \theta$, where γ is the Lorentz factor of the electron, B is the magnetic field strength, θ is the pitch angle between the electron's velocity and the magnetic field, and K_1 is a constant defined by Pacholczyk (1970, eq. [3.32]). Two key characteristics of the energy loss rate due to synchrotron radiation are displayed in this relation: the rate is strongly dependent upon the electron energy and the component of the magnetic field perpendicular to the electron velocity.

The emission spectrum from a single particle peaks near a frequency given by $K_2 \gamma^2 B \sin \theta$, where K_2 is given by Pacholczyk (1970, eq. [3.28]). The spectrum below this frequency behaves as a power law of index $\frac{1}{3}$, while above this frequency the spectrum drops off exponentially. The emission from an ensemble of electrons can be calculated by convolving the emission spectrum per electron with the energy distribution spectrum of the ensemble. The power-law spectra observed for extragalactic radio sources encourages examination of power-law energy distributions of electron energy. A power-law distribution in energy of index S , $N(E) \propto E^S$, results in a power-law emission spectrum, $I_\nu \propto \nu^\alpha$, with the power-law index given by $\alpha = (S + 1)/2$. Typical observed spectral indices of -0.75 in radio galaxies will then arise from energy distribution indices of -2.5 .

Of great physical importance is the evolution of the spectrum with time. Synchrotron radiation losses deplete the highest energy electrons first, leading to a steepening of the emission spectrum at high frequency over time. A study of spectral steepening at high frequency in radio sources yields information on the radiative lifetimes of the particles, and hence may yield information on source dynamics. Although synchrotron losses will always lead to a steepening in the spectrum at high frequency, the form of the high-frequency steepening and the physical interpretation of the distribution depend on the evolution of energy input into the relativistic electrons and on the evolution of the pitch-angle distribution. Kardashev (1962) and Pacholczyk (1970) have solved the equation of energy continuity for an ensemble of synchrotron-radiating electrons for numerous situations of physical interest. We refer to their work below.

We consider the evolution of the emission spectrum from a particle distribution that is initially power-law in energy and isotropic in pitch angle and resides in a magnetic field which is isotropically tangled on scales much smaller than the spatial resolution element. We consider three distinct evolutionary models, which we designate as CI, JP, and KP (see also Myers & Spangler 1985). In each case, the spectral break frequency above which the spectrum steepens from the injected power law, relates to physical quantities through the equation

$$t_s = 1610 B^{-3/2} \nu_B^{-1/2} \text{ Myr} . \quad (1)$$

In this equation, the "synchrotron age" of the distribution, t_s , is simply the time since the spectrum was a power law out to infinite frequency (i.e., the time since the process began). The magnetic field, B , is in μG , and the break frequency, ν_B , is in GHz. The models differ in the form of the high-frequency

falloff, which depends on a number of physical processes in the evolution of the particle distribution.

The JP (Jaffe-Perola) and KP (Kardashev-Pacholczyk) models incorporate a “one-shot” injection of a power-law distribution of electrons in time, with no further particle injection (Jaffe & Perola 1973; Kardashev 1962; Pacholczyk 1970; see Myers & Spangler 1985 for a summary). The JP model allows for continuous isotropization of the pitch-angle distribution with time, i.e., scattering in pitch angle on time scales much smaller than the radiative lifetime of the particles. This leads to a sharp cutoff in the electron energy distribution and, hence, to an exponential cutoff in the emission spectrum. The KP model allows for no pitch-angle scattering of the relativistic particles. Hence, particles will maintain their initial pitch angle over time, since synchrotron radiation itself has no effect on pitch angle. The distribution will develop a high-energy “tail” of particles at oblique pitch angles. The resulting emission spectrum steepens above the break to a new power law, with an index that depends on the injected power-law index as: $(4/3)\alpha_{in} - 1$, where α_{in} is the injected power-law spectral index.

The CI (continuous injection) model includes the continuous injection of a power-law distribution of relativistic electrons. This model was first developed for the case of an unresolved source, for which we see all the particles all the time. The observed spectrum for this situation is then the sum of the emission from the various electron populations at different synchrotron ages, ranging from zero to the age of the source ($= t_s$). The flux density at frequencies below the synchrotron “break” rises with time, since new particles are constantly being added. Above the synchrotron break, the spectrum steepens from the low-frequency (injected) power law to a different power law with a spectral index steeper by $-\frac{1}{2}$ (assuming the injection rate is constant in time). The high-frequency steepening is essentially independent of whether the particles age according to the JP or the KP model, since the emission at high frequency is dominated by the newly injected particles.

For spatially resolved objects, Meisenheimer et al. (1989) and Heavens & Meisenheimer (1987) show that the CI model will apply when there exists within the telescope beam a small zone of continuous high-energy particle injection (e.g., a shock front), and synchrotron-radiating outflow from this region. In this case, a steady state is reached where the break frequency and the low-frequency surface brightness remain constant with time, since particles are flowing out of the telescope beam. The synchrotron age, as measured from the spectral break frequency and the magnetic field, then relates simply to the outflow distance divided by the outflow velocity (see Fig. 7 and eq. [8] in Meisenheimer et al. 1989), and the outflow distance is determined essentially by the angle subtended by the telescope beam and the distance to the radio source. Implicit in this model is the assumption that the field strength is the same in the region where the particles are injected as in the outflow region. If the field strength drops dramatically during outflow on a distance scale that is much smaller than the beam size, then the distance to use in the velocity calculation is the size scale over which the fields are of roughly uniform (and large) strength. It is also implicit in the Meisenheimer et al. (1989) model that the outflow is symmetric with respect to the jet axis. We apply this model to the hot spots in Cygnus A in § 5.1.2.

Each of these spectral models—CI, KP, JP—can be characterized by an injection index (α_{in} = power-law index at frequencies below the synchrotron break) and a “break

frequency” (ν_B) above which the spectra steepen from the injected power law, and by their behavior at frequencies above the synchrotron break. The CI and JP models can be thought of as limiting cases. The high-frequency steepening of the CI model is the least expected from synchrotron losses, while the exponential cutoff of the JP model is the fastest that a synchrotron spectrum can steepen. The KP model falls in between. The goal of a multifrequency analysis of nonthermal radio continuum emission is to determine the values of α_{in} and ν_B and the behavior of the spectrum above the break.

Examples of the three models—CI, KP, JP—are shown in Figure 1. The frequency axis has been normalized by the break frequency in each case. Evident is the large range over which curvature is significant—almost two orders of magnitude in frequency. Also evident are the large differences among the models above the break. Multifrequency observations over a broad range in frequency are thus needed to differentiate among these models, in particular at frequencies above the spectral break.

2.2. Expansion, Reacceleration, and Other Difficulties

Realistic models must include other physical effects, the most important of which is likely to be adiabatic expansion losses. Expansion losses cause a decrease in particle energies and magnetic field strengths. The net effect is to cause a scaling of the synchrotron emission spectrum, in both frequency and flux density. This implies a simple translation of the spectrum in the log plane (Scheuer & Williams 1968). Adiabatic expansion losses shift the bend in the spectrum to lower frequencies, thus mimicking synchrotron losses. The difference between expansion losses and synchrotron losses is seen at low frequency. Synchrotron losses have virtually no effect below the break frequency, while expansion losses cause a large decrease in the low-frequency flux density. This difference is demonstrated in Figure 2. The solid curve is a KP spectrum observed at time t_0 . This spectrum is then aged by a factor of 5, assuming only synchrotron losses. Synchrotron losses cause a migration of the break frequency to lower frequencies, with virtually no

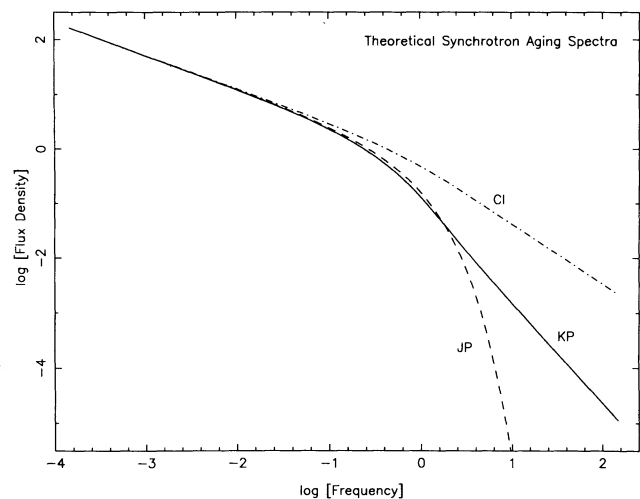


FIG. 1.—Examples of the three spectral models CI, KP, and JP. The frequency axis has been normalized by the break frequency. The dot-dash line is the CI (continuous injection) model, the dashed line is the JP (Jaffe-Perola) model, and the solid line is the KP (Kardashev-Pacholczyk) model.

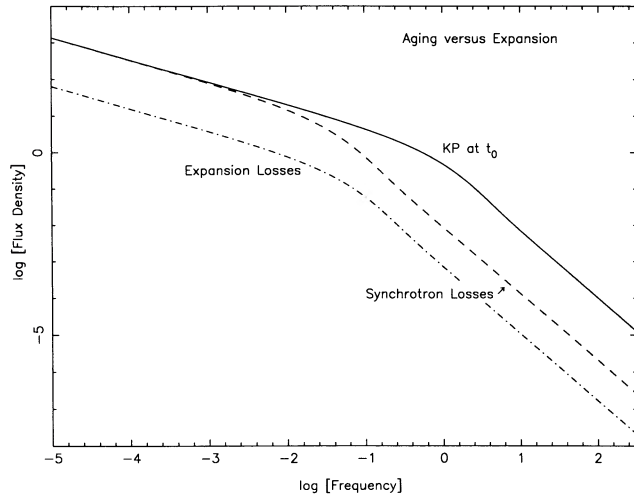


FIG. 2.—Example showing the effect of synchrotron aging and adiabatic expansion losses. The solid line shows a KP model spectrum at time t_0 . The dashed line shows the same distribution aged by a factor of 5, assuming energy losses only through synchrotron radiation. The dot-dash line shows the original distribution after an adiabatic expansion by a factor of 2, with no synchrotron losses. The frequency axis is in units of the break frequency for the distribution at time t_0 .

change occurring below the break. Taking the same initial spectrum, and allowing for losses due to a spherical expansion by a linear factor of 2, with no synchrotron losses, causes a decrease in both the break frequency and the low-frequency flux density. Hence the two phenomena (synchrotron losses and expansion losses) can be separated by comparison of the spectral evolution at low frequency.

A second potentially important effect is in situ particle reacceleration. Particle reacceleration is a different process than continuous particle injection. In the continuous injection model, the total number of radiating particles is given by the product of the injection rate and the time since the process began. Reacceleration alters an existing particle distribution, hence the total number of particles is constant. If the reacceleration process is weak and localized, then the effect will probably be seen only at high frequencies, lessening the degree of high-frequency spectral steepening. If reacceleration is strong and universal, then the entire particle spectrum will be altered, and the measured break frequency no longer relates to the time since the particles were initially injected into the source. An example of the evolution of the particle spectrum including a power-law injection, synchrotron losses, and stochastic particle reacceleration is given by Kardashev's (1962) paired process 2.

Third, there are energy losses due to inverse Compton scattering off the cosmic background radiation. For Cygnus A, inverse Compton losses can be ignored, since the energy density in the magnetic fields in the lobes (assuming minimum-energy conditions) is a factor of 200 greater than that in the microwave background.

Last, there is the question of whether the injected spectrum is power-law. Again, such an assumption is supported by the observed power-law nature of the integrated spectra of radio galaxies. Given adequate spectral coverage, one can turn the question around and use the data to test the assumption of power-law injection. We discuss the possibility of curvature in the injection spectrum in the context of the jet model for radio galaxies in § 5.2.2.

Overall, there are a number of caveats to keep in mind when considering aging and velocity calculations based on observed break frequencies. First, if expansion losses are important, then the age derived from the observed break frequency is greater than the true radiative lifetime of the distribution. Second, if in situ particle acceleration is important, then the age derived from the spectral break may be smaller than the true age of the population. Last, velocity calculations depend on distances across the lobes, which, in turn, depend on the angle of the source relative to the sky plane. In this paper we assume that Cygnus A is close to the sky plane (Hargrave & Rule 1974), and that $H_0 = 75 \text{ km s}^{-1} \text{ Mpc}^{-1}$, which gives a scale of $1'' \approx 1 \text{ kpc}$.

2.3. Minimum-Energy Fields

Another very large uncertainty in a synchrotron aging analysis is the magnetic field strength. Equation (1) shows that the spectral age depends more strongly on the field than on the break frequency ($t_s \propto B^{-3/2} v_B^{-1/2}$). Unfortunately, no method presently exists with which to determine the magnitude of the field in the lobes of powerful radio galaxies. A further difficulty is that, if the field strength has varied over time, then the age calculation requires the use of a weighted mean field (see § 5.1). Most synchrotron spectral aging studies to date assume magnetic field strengths which minimize total energy density in relativistic particles and fields. Although the minimum-energy assumption is highly uncertain (Leahy 1990), we assume minimum-energy fields in Cygnus A for our age calculations below, for lack of a better estimate. The effect of spatial and temporal field variations on spectral aging analyses of radio sources has been discussed by Wiita & Gopal-Krishna (1990) and Siah & Wiita (1990), and are considered further in § 5.1.1 below.

The minimum-energy calculation involves a number of assumptions, as outlined in Miley (1980). We assume filling factors of 1, equal energies in relativistic particles and fields, and upper and lower cutoff frequencies of 0.01 and 100 GHz. Minimum-energy calculations are insensitive to the cutoffs. We assume magnetic fields tangled on scales much smaller than our resolution element. Such a field configuration implies that the "effective" magnetic pressure (including the tension term) is $\frac{1}{3}$ times the magnetic energy density. In this case, the total pressure in relativistic particles and fields is simply $\frac{1}{3}$ times the total energy density, and minimizing total pressure rather than energy yields the same result for both fields and pressures as minimizing total energy density.

For the hot spots we calculate fields from the observed surface brightnesses on a 15 GHz image, at $0''.1$ resolution (Carilli et al. 1989a), assuming a disklike geometry and a spectral index of -0.5 . Minimum-energy fields vary from 250 to 350 μG on the high surface brightness structures in the hot spots. We use a value of 300 μG for most of the hot spot calculations in this paper. The corresponding minimum pressure is $2.8 \times 10^{-9} \text{ dynes cm}^{-2}$.

For the lobes we calculate minimum-energy fields from the observed surface brightness on a 327 MHz image at $4''.5$ resolution. We assume a cylindrical geometry, with a width given by the observed source width, and we use a spectral index of -0.7 . We find that the fields vary from about 65 μG at the ends of the lobes farthest from the core, down to about 45 μG in the center of the radio source. Corresponding pressures are 1.3×10^{-10} and $6.3 \times 10^{-11} \text{ dynes cm}^{-2}$, respectively. The lobes are composed of much filamentary substructure (Perley et al. 1984). Minimum-energy fields in these structures

TABLE 1
OBSERVING LOG

Date	Array	Frequency (MHz)	Bandwidth (MHz)
1980 Feb 24	Mixed	1446, 4886	12.5
1982 Jun 20	A	1446, 4886	6.25
1982 Oct 25	B	1446, 4886	12.5
1982 Oct 28	B/D	1446, 4886	12.5
1983 Feb 2	C	4886	50
1983 Sep 15	A	14400, 14650, 14950, 15300	6.25
1983 Oct 23	A	4525, 4995	6.25
1984 Jan 14	B	4525, 4995, 14655, 14945	12.5
1984 Jan 23	B	4525, 4995, 14655, 14945	12.5
1984 Apr 15	C	4525, 4995, 14655, 14945	12.5
1984 Apr 23	C	14655, 14945	12.5
1984 Apr 24	C	14655, 14945	12.5
1984 May 19	C	14655, 14945	25
1984 May 24	C	14655, 14945	12.5
1984 Aug 28	D	4525, 4995, 14655, 14945	25
1986 Sep 3	B	327, 1345, 1704	3.13, 6.25, 3.13
1986 Dec 1	C	327, 1345, 1704	3.13, 6.25, 3.13
1986 Dec 1	C	14635, 14985, 15085, 15145	50
1987 Mar 24	D	14635, 14985, 15085, 15145	50
1987 Aug 18	A	327, 1345, 1704	3.13, 6.25, 3.13
1987 Sep 1	A	327, 1345, 1704	3.13, 6.25, 3.13
1989 Nov 11	D	22485	50

could be about a factor of 1.15 to 2 times larger than the “mean” fields calculated above, depending on whether the filaments are ropelike or sheetlike. Hence, these structures are overpressed by factors of 1.3–4 with respect to their environs (depending on geometry), if minimum-energy conditions apply.

3. OBSERVATIONS AND SPECTRAL MODEL FITTING

3.1. Observations and Errors

We observed Cygnus A at a number of radio frequencies using multiple configurations of the Very Large Array (VLA) radio synthesis imaging telescope of the NRAO. Table 1 shows an observing log for the VLA observations. We also include a low-frequency (0.151 GHz) image made with MERLIN (Leahy, Muxlow, & Stephens 1989). Data for the hot spots above 22 GHz were taken from the literature.

Standard VLA phase and amplitude calibration was employed. Our flux density scale at each frequency was set with observations of 3C 286, and was checked with observations of 3C 48. Images were deconvolved using the CLEAN algorithm, and residual antenna-based errors were minimized through self-calibration (see Perley 1988). The final dynamic range on each image is better than 1000/1 (peak to off-source rms).

Table 2 lists the estimated flux density errors in our data at 4.5 resolution, at each frequency. Column (2) gives the additive error, as given by the measured off-source rms. Column (3) gives the multiplicative error, which includes an estimate of errors in the flux density bootstrapping procedure and an estimate of errors due to deconvolution. When fitting spectral models to the data, the additive and multiplicative errors were added in quadrature. Flux bootstrapping errors were estimated by comparing the integrated flux density of Cygnus A on the deconvolved VLA images to single-dish measurements (Baars et al. 1977). Deconvolution errors were estimated by comparing images deconvolved using the CLEAN algorithm (Clark 1980) with those deconvolved using the maximum-entropy algorithm (Cornwell & Evans 1985). We have not

included the contribution from “self-noise” in regions of high surface brightness (Anantharamiah 1988) for the reason that our images are dynamic-range-limited. The measured “noise” for each of our images results from imperfections in the imaging process, and is at least an order of magnitude larger than the expected “self-noise” on the hot spots at 4.5 resolution.

3.2. Spectral Model Fitting

The three spectral aging models, CI, KP, and JP, were fitted to multifrequency data for images at 4.5 and 1.5 resolution. At 4.5 resolution we have data at nine frequencies ranging from 151 MHz to 22 GHz. At 1.5 we have data at six frequencies ranging from 1.35 to 15 GHz. The variables in the spectral fitting process were the injection index, the break frequency, and the intensity scaling.

The spectral fitting routine requires a multifrequency “cube” of images of equal resolution and geometry, and a file containing frequency and error information. The program then fits the chosen spectral model to the observed data at each pixel in the image. The user sets a “blanking” surface brightness level for each frequency, below which data at that fre-

TABLE 2
FREQUENCIES AND ERRORS

Frequency (MHz) (1)	Additive Error (mJy beam ⁻¹) (2)	Multiplicative Error (percent) (3)
151.....	...	8
327.....	230	6
1350.....	40	3
1450.....	37	2
1704.....	70	4
4525.....	20	2
4995.....	15	2
14900.....	15	3
22450.....	25	5

quency are ignored. Blanking greatly speeds up the process, since fitting is then done using only data of high reliability. The user also sets a minimum number of frequencies allowed in the fit, below which the program skips the position completely, setting all the output parameters to magic "blank" values. The program also allows for the "blanking" of output values for pixels where the resulting break frequency falls well outside the observed frequency range, since in these regions the results are highly unreliable.

For Cygnus A, we set a blanking level at each frequency of 5 times the measured off-source rms, and a minimum number of frequencies allowed for fitting of 5. We also blanked output values at pixels for which the measured break frequency was a factor of 5 below the minimum frequency in the data, or a factor of 5 above the maximum frequency in the data.

The program includes a Myers & Spangler (1985) two-

frequency fit for a first guess at the break frequency. The Myers & Spangler routine has the advantage of being independent of the intensity scaling, and should provide a first guess for ν_B near the global minimum in χ^2 space.

The output of the program is in the form of images of the various fit parameters. The program also creates images of reduced χ^2 , and the formal error in break frequency. When discussing χ^2 results, we use as a criterion for a "reasonable" fit a Q -test limit of 0.05 (Meyer 1975).

4. IMAGES AND ANALYSIS

4.1. Images of Total Intensity

Figure 3 shows two images of total intensity of Cygnus A, one at low frequency (327 MHz) and one at high frequency (15 GHz), both at $4''.5$ resolution. A number of features have been

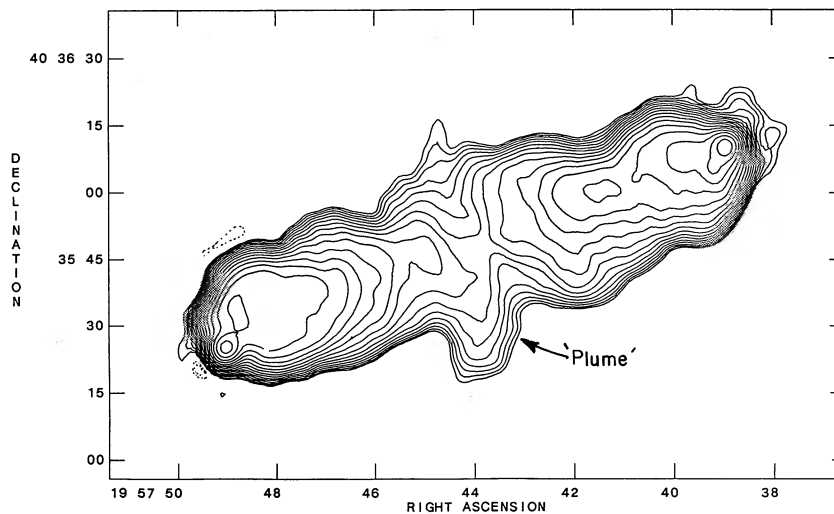


FIG. 3a

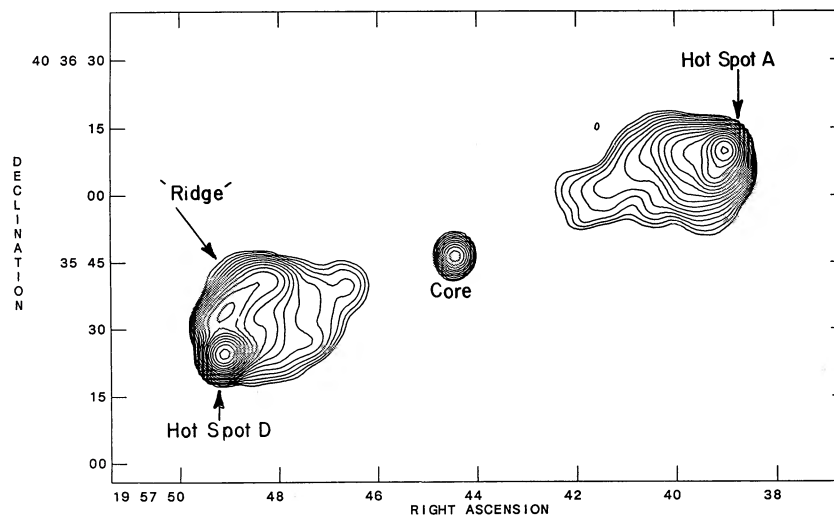


FIG. 3b

FIG. 3.—(a) Image of Cygnus A at 327 MHz, $4''.5$ resolution. The contour levels are a geometric progression in the square root of 2, such that an interval of 2 contours implies a change in surface brightness by a factor of 2. The contour levels are $-1.3, -0.9, 0.9, 1.3, 1.8, 2.5, 3.6, 5.1, 7.2, 10.2, 14.4, 20.4, 28.8, 40.7, 57.6, 81.5, 115,$ and 163 Jy beam^{-1} . The peak surface brightness on the image is 212 Jy beam^{-1} . A few features have been labeled for reference in the text. (b) Image of Cygnus A at 15 GHz, $4''.5$ resolution. Again, the contours are a geometric progression in the square root of 2. The contour levels are $-0.05, 0.05, 0.07, 0.1, 0.14, 0.2, 0.28, 0.4, 0.57, 0.8, 1.1, 1.6, 2.3, 3.2, 4.5, 6.4, 9.1, 12.8,$ and $18.1 \text{ Jy beam}^{-1}$. The peak surface brightness is $21.2 \text{ Jy beam}^{-1}$. A few features have been labeled for reference in the text.

labeled for reference. Also, for reference, we use Np to designate the northwestern radio lobe, and Sf to designate the southern radio lobe.

A prominent feature at low frequency is the “bridge” of radio emission, of fairly constant width and surface brightness, extending the entire length of the source. Near the center of the bridge are two “plumes” of emission extending to the north and south. Such plumes are common in powerful radio galaxies, and may arise from back-flowing lobe material, which is deflected away from the high-density and high-pressure regions near the center of the associated galaxy (Leahy & Williams 1984).

At high frequency, the dominant features are the radio core and the hot spots (designated A and D by Hargrave & Ryle 1974). The radio bridge and plumes, prominent at low frequency, are absent at high frequency. Another interesting feature in the high-frequency image is the bright “ridge” of emission to the north of hot spot D in the southern lobe. This feature was designated F by Alexander, Brown, & Scott (1984). At higher resolution, the structures along this feature are complex, both in total and in polarized intensity (Dreher et al. 1987a).

4.2. Hot Spot Spectra

The flux densities for hot spots A and D at 4''5 resolution are given in Table 3. A resolution of 4''5 is sufficient to isolate the hot spots from the rest of the lobes, and yet include all of the high surface brightness structure seen at 15 GHz, 0''1 resolution (Carilli et al. 1989a). Observations above 22 GHz were made with spatial resolutions lower than 4''5. For these data we have estimated the contribution from the surrounding source structure to the hot spot peaks at the observed resolutions, and removed this contribution. The error bars include these estimates of contamination.

Figure 4 plots the spectral data for each hot spot. The solid curves are the resulting best fits for the continuous injection

TABLE 3
HOT SPOT FLUXES AT 4''5 RESOLUTION AND SPECTRAL
MODEL FIT RESULTS

FREQUENCY (MHz)	PEAK SURFACE BRIGHTNESS (Jy beam ⁻¹)	
	Hot Spot A	Hot Spot D
151	275 ± 22	237 ± 19
327	212 ± 13	196 ± 12
1350	99 ± 3	110 ± 3
1450	93 ± 2	104 ± 2
1704	84 ± 4	97 ± 4
4525	40 ± 1	53 ± 1
4995	38 ± 1	50 ± 1
14900	13.8 ± 0.7	21 ± 1
22485	8.9 ± 0.5	15 ± 1
89000 ^a	1.9 ± 0.2	4.2 ± 0.5
230000	0.72 ± 0.1	1.3 ± 0.14
273000	0.69 ± 0.15	1.2 ± 0.1
375000	0.65 ± 0.16	1.1 ± 0.2
ν_B	12 ± 1 GHz	6.5 ± 0.7 GHz
α_{in}	-0.55 ± 0.09	-0.50 ± 0.09
χ^2 (reduced)	0.63	0.62
ν_{co} (LEC) ^b	220 ± 20 MHz	190 ± 20 MHz
ν_1 (SSA) ^c	160 ± 10 MHz	170 ± 10 MHz

^a References to data above 22 GHz are given in the caption to Fig. 4.

^b Low-energy cutoff.

^c Synchrotron self-absorption.

model. The parameters resulting from the spectral model fitting are given in Table 3. The data are well fitted by the CI model ($\chi^2 = 0.6$ for both spots), and the spectral break frequency is around 10 GHz for each hot spot, with formal errors in ν_B from the fitting process of about 10%. For each hot spot we find an injection index near -0.5 .

We have also fitted both a JP and the KP model spectrum to the data, and find that neither of these models fits well. Both models result in very large break frequencies (~ 300 GHz), leaving a simple power law over most of the observed frequency range, with a best-fit index of -0.6 . This implies that the high-frequency steepening in the data is much smaller than required by either the KP or the JP spectrum. Hence, the spectral fitting program tries to fit the data with a straight line by pushing the break frequency to the high edge of the observed frequency range.

The data at 327 and 151 MHz fall well below the low-frequency power law of the best-fit CI model. In order to estimate whether this low-frequency flattening affects the calculation of the injection index and other parameters above, we have fitted spectra excluding data at frequencies below 4.5 GHz. The result is no significant change in either α_{in} or ν_B . Hence, the CI model is well constrained by the higher frequency data, and in particular by the fact that the hot spot spectral data between 10 and 400 GHz (i.e., above the break frequency) are very well fitted by a power law of index -1.0 . Hence, we consider the flattening of the hot spot spectra below 327 MHz to be a phenomenon separate from synchrotron aging. The fit parameters given in Table 3 were obtained without the two low-frequency points in the fit.

Two possible causes for such a low-frequency flattening are synchrotron self-absorption or a low-energy cutoff in the electron energy spectrum. We have fitted model spectra including these effects to the data, and the results are shown for hot spots A and D in Figures 4c and 4d, respectively, and summarized in Table 3. The low-energy cutoff spectrum fits the data reasonably well ($\chi^2 = 0.3$), while the synchrotron self-absorption model fits the data poorly ($\chi^2 = 2$). We discuss these results, and other possible explanations for the low-frequency flattening of the hot spot spectra, in § 5.4.

4.3. Lobe Spectra

4.3.1. Expansion Losses in the Radio Lobes

Figures 5a and 5b show spectral data for five positions in the northern lobe and four positions in the southern lobe, respectively. The solid lines simply connect the data points with straight lines. The spectrum labeled 1 in each plot corresponds to the hot spot in each lobe. The spectra labeled 2–5 are for lobe positions situated along a line joining the hot spot and the core, with each position separated by 9''. The distance from the hot spot is indicated on each curve. We plot emissivities as calculated from observed surface brightnesses, assuming a cylindrical geometry for the lobes and a spherical geometry for the hot spots.

The large drop in emissivity at frequencies below 5 GHz going from position 1 to position 2 may signal large expansion losses going from the hot spots to the lobes. We discuss this possibility in §§ 5.1 and 5.2.

A much smaller drop at frequencies below 5 GHz is seen going from position 2 to position 3, while for positions 3, 4, and 5 the low-frequency parts of the spectra are coincident. The

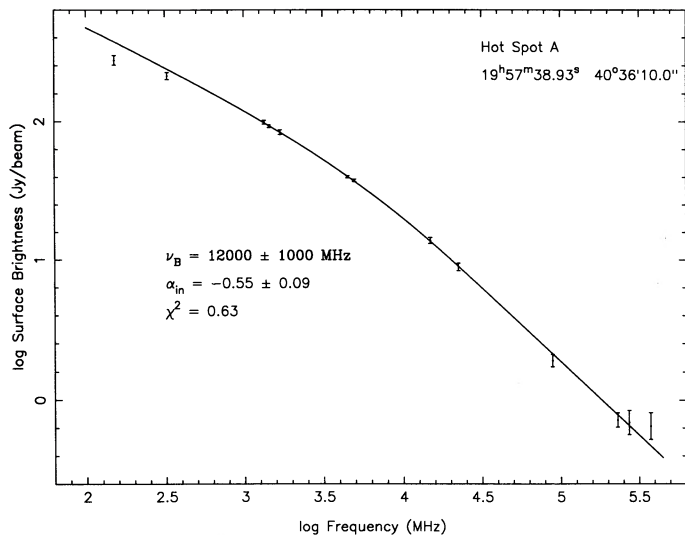


FIG. 4a

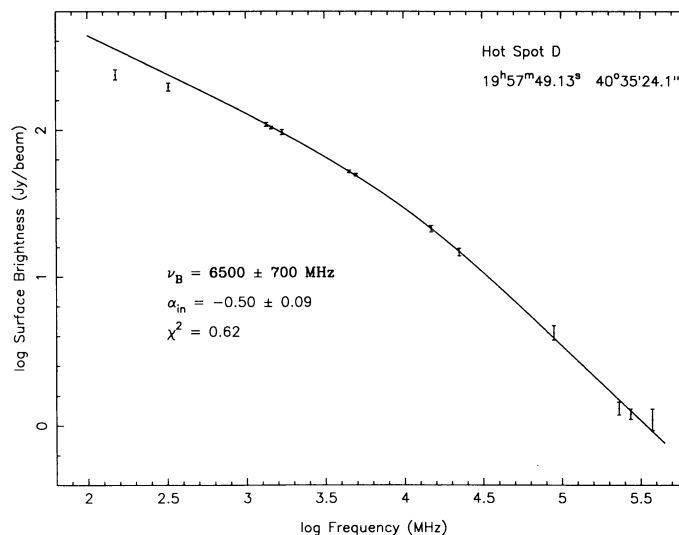


FIG. 4b

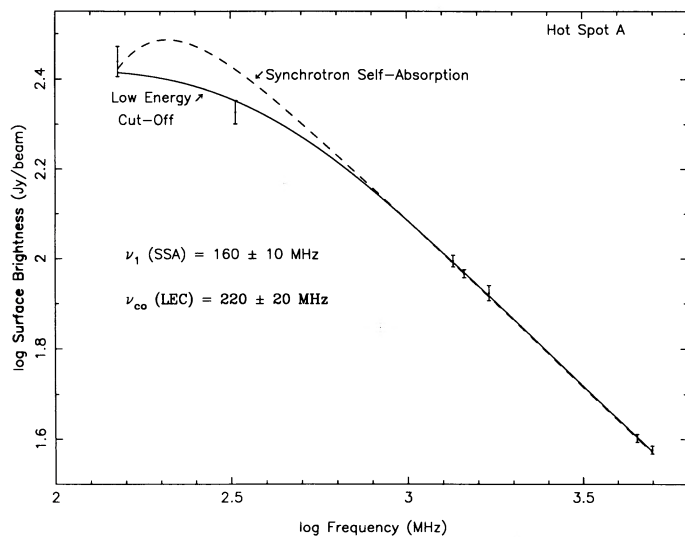


FIG. 4c

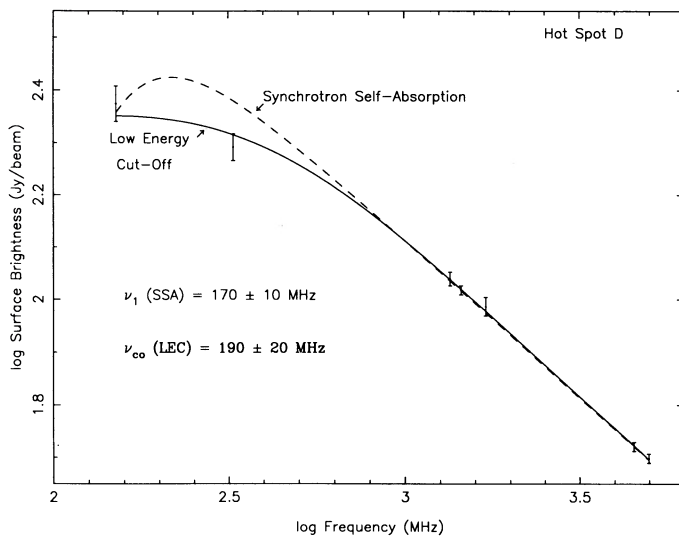


FIG. 4d

FIG. 4.—(a) Spectral data for hot spot A at the end of the northern lobe, at $4''$ resolution. The solid line is the best-fit CI spectral model, and the parameters for this fit are listed on the plot and also in Table 3. Data above 22 GHz are from Wright & Birkinshaw (1984), Eales et al. (1989), Salter et al. (1989), Hobbs et al. (1978), and Fogarty et al. (1971). (b) Same as (a), but for hot spot D at the end of the southern lobe. (c) Same as (a), but showing only the low-frequency data. The solid line is the emission spectrum from a power-law distribution of electrons with a low-energy cutoff. The dashed line is a synchrotron self-absorbed spectrum. The resulting model parameters are listed on the plot and also in Table 3. The relationship between the cutoff frequency (as listed on the plot) and the cutoff energy is discussed in § 5.4. (d) Same as (c), but for hot spot D.

spectra in these positions differ only at high frequency. This indicates that there is a mechanism, such as synchrotron radiation, which preferentially removes the high-energy electrons in the radio lobes. The simple scaling law implied by expansion losses, or the related effect of a changing magnetic field, cannot account for this observed behavior. This implies that the dominant energy loss mechanism in the lobes of Cygnus A is synchrotron radiation.

4.3.2. Results from Spectral Model Fitting

We have fitted both the KP and the JP model spectrum to the observed multifrequency data at each position in the radio lobes. The spectral data for a few selected points in the lobes are shown in Figures 6a–6f. The solid and dashed lines are the

best-fit KP and JP models, respectively. The positions for each point, and the resulting fit parameters, are given on each figure.

The results for the spatial distribution of the injection index are similar for both the KP and the JP model. In both cases, the distribution is fairly uniform across the lobes, with a mean value of -0.7 ± 0.1 . There is no indication for increasing injection index with distance from the hot spots, which implies that our frequency coverage is adequate to avoid biasing toward low injection index in regions of low break frequency. We adopted the value of -0.7 for subsequent analysis.

Figure 7a shows the distribution of break frequency across the lobes of Cygnus A at $4''$ resolution, as found for the KP model. Results for the distribution of ν_B for the JP model are similar and are not displayed. Formal errors on the values for

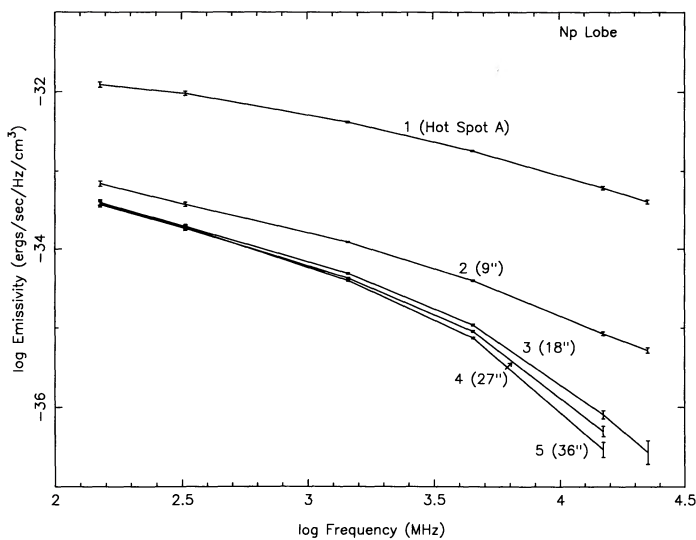


FIG. 5a

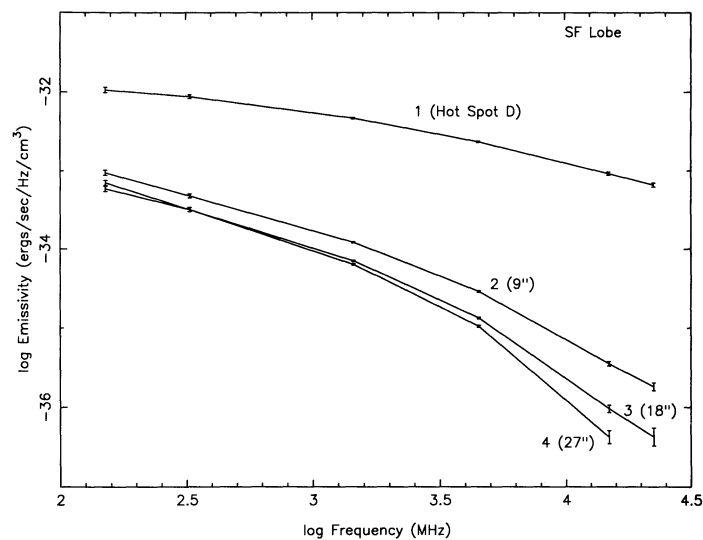


FIG. 5b

FIG. 5.—(a) Spectral emissivity at 4.5 resolution at five locations in the northern lobe. Spectrum 1 is for hot spot A. Spectra 2–5 are taken at positions situated along a line connecting the hot spot and the core, with 9" between positions. Each spectrum is labeled with the corresponding distance from the hot spot. The emissivity is calculated assuming a cylindrical geometry for the lobes. The solid lines simply connect the data points. (b) Same as (a), but for the southern lobe.

ν_B range from about 5% to 10%. There is a clear trend for decreasing break frequency with distance from the hot spots; falling from 50 GHz or above near the hot spots, down to a minimum of 750 MHz in the southern plume.

Although the values of ν_B and α_{in} are similar for the KP and JP models, there is a very clear difference between the two models on the images of χ^2 . The values of reduced χ^2 for the KP model range from 0.3 to 3 in the lobes, implying reasonable agreement between model and data in most regions of the source. The values for reduced χ^2 for the JP model range from 2 to 20 in the lobes, implying poor agreement between model and data over most of the lobes. The cause for the poor fit of the JP model is that the data show a more gradual steepening at high frequency than the exponential cutoff required by the JP model. This behavior can be seen in the examples of Figure 6.

The lack of a high-frequency exponential cutoff in the radio lobe spectra has important physical consequences (see § 5.2.1), so it is important to ensure that the effect is not due to observational limitations. In this context, the most important observational limitation is beam smearing. The smearing by the beam of small-scale regions of different break frequencies will tend to smooth out any sharp spectral break, and might make a JP spectrum look like a KP spectrum. We feel that this explanation is unlikely for two reasons. First, simple tests on model data show that to smooth a JP model spectrum into a KP model spectrum requires at least a factor of 4 spread in break frequency within the beam (given the observed wavelength range and typical break frequencies in the source). Such large gradients in ν_B are not seen in the radio lobes, except in a few isolated regions, such as just outside of the hot spots. Second, a high-resolution (0.4) spectral index image between 5 and 15 GHz shows that the spectral index has a fairly constant value of -2 over most of the tails of the radio lobes (i.e., in regions with $\nu_B \leq 5$ GHz), and that it never gets below this value. Such a morphology is consistent with the KP model, which predicts a power-law spectrum above the break of index -2 , for an injection index of -0.7 . This essentially rules out spatial

smearing across the 4.5 restoring beam as the cause for the lack of a high-energy exponential cutoff in the lobe spectra.

There is still the possibility that back-front dilution is smearing the JP model into the KP model, especially in the light of the observed gradients in ν_B from the center to the edges of the radio lobes (see § 5.1.1 and Fig. 7a). Although we cannot rule this out, we feel it unlikely, since there is no evidence for decreasing χ^2 along the edges of the radio lobes for the JP model, where back-front dilution is less important. A test of this possibility would be to observe at higher frequencies (≥ 22 GHz), with the prediction that the spectra will eventually show an exponential cutoff.

Figure 7b shows an image of ν_B at 1.5 resolution. The higher spatial resolution of this image allows inspection of the spectral behavior on specific source structures in greater detail. However, the limited spectral range at this resolution (1.35–15 GHz) implies an undersampling of the break in the spectrum. Given this undersampling, no fitting was done for the low-frequency spectral index. We assume the value of -0.7 , as determined from our spectral analysis at 4.5 resolution. In Figures 7c and 7d the break frequency contours for the north and south lobes, respectively, are superposed on images of total intensity at 6 cm.

Of great physical interest is the radio spectrum of the filamentary structures in the radio lobes (Perley et al. 1984). From Figures 7c and 7d, it appears that the brighter filaments have higher break frequencies than their environs by about 20% or so. A comparison of a series of cuts made through the lobes in both total intensity and break frequency confirms the correlation between higher break frequency and total intensity. If the filaments are ropelike, then a proper spectral analysis must remove the contribution from any diffuse component. This process is difficult, since the contrast between most filaments and their environs is less than about 30%, and since the diffuse emission of the lobes is not of uniform surface brightness but shows gradients both across and along the radio lobes. We have tried to determine the spectrum of the peak of the most prominent filament in the tail of the northern lobe (position of

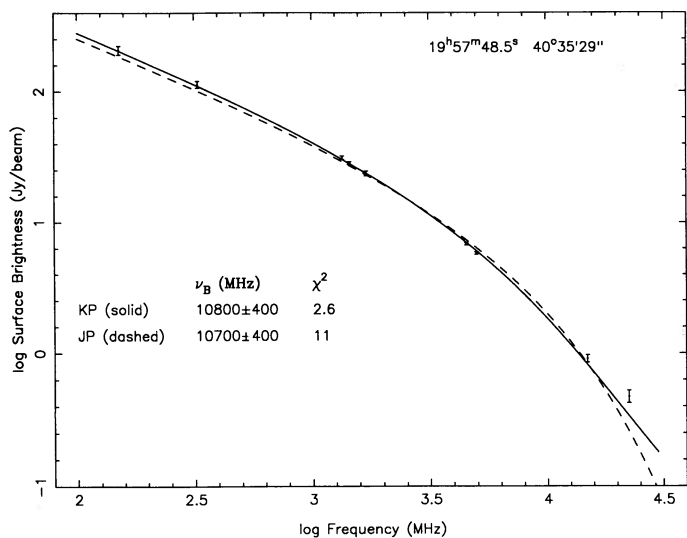


FIG. 6a

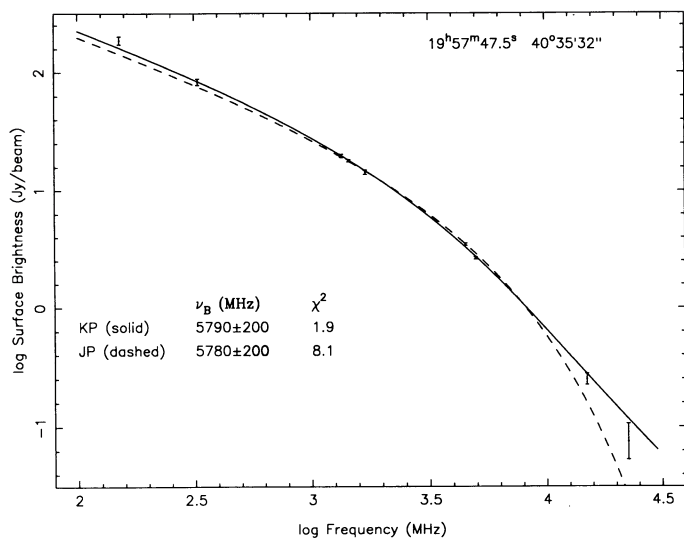


FIG. 6b

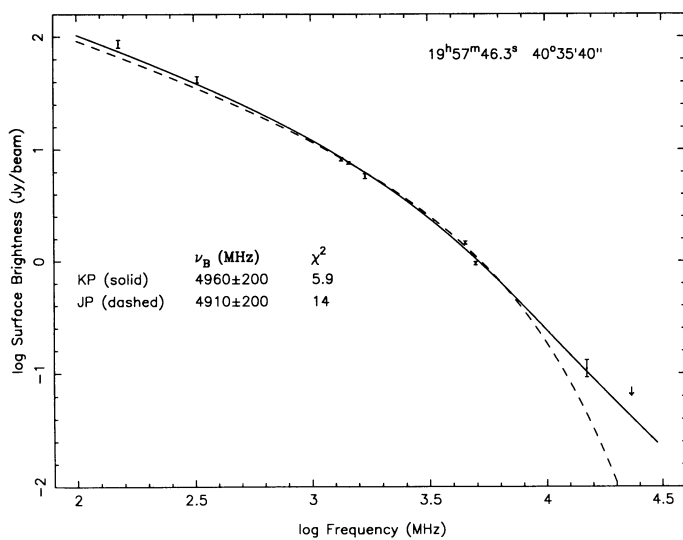


FIG. 6c

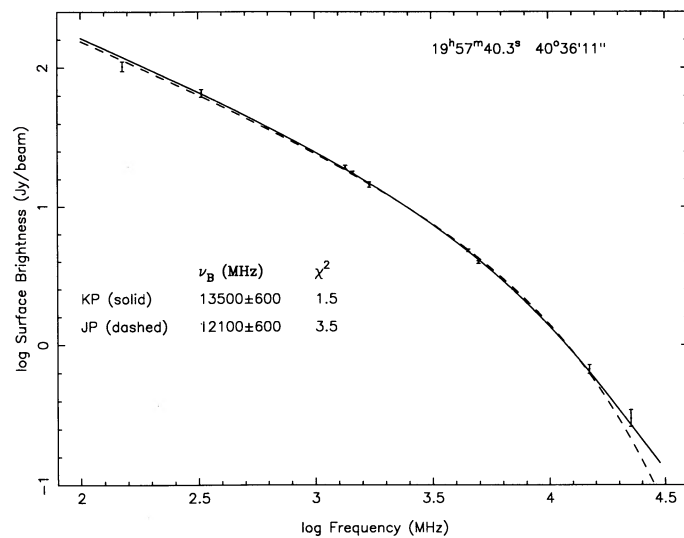


FIG. 6d

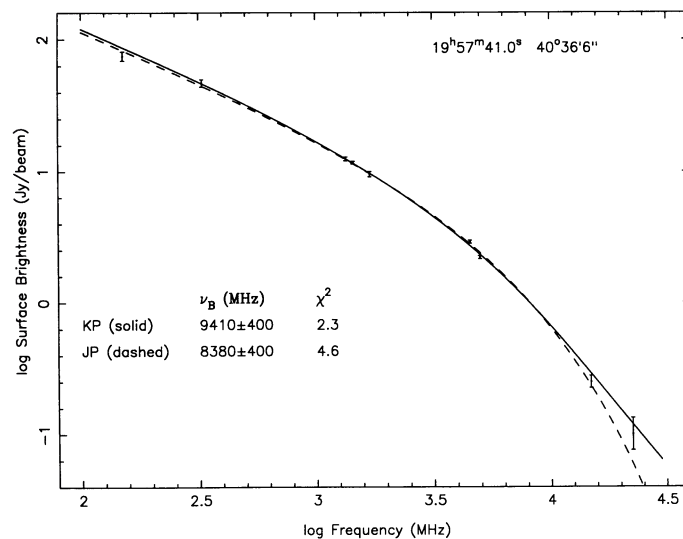


FIG. 6e

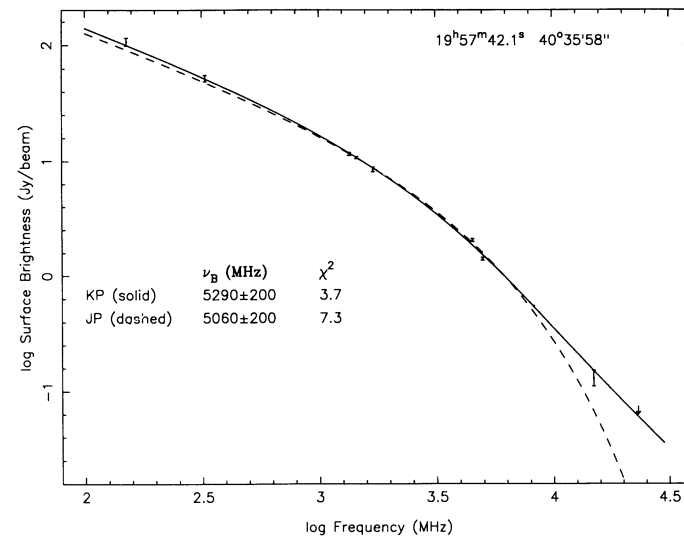


FIG. 6f

FIG. 6.—Examples of observed spectra and spectral model fit results for a number of positions in the radio lobes. Data are at $4''$ resolution. The solid lines are results from the KP model, while the dashed lines are results from the JP model. All fits use $\alpha_{\text{in}} = -0.7$. Listed on each plot are the position in the source (B1950) and the results from the spectral model fitting for the break frequency and the reduced χ^2 .

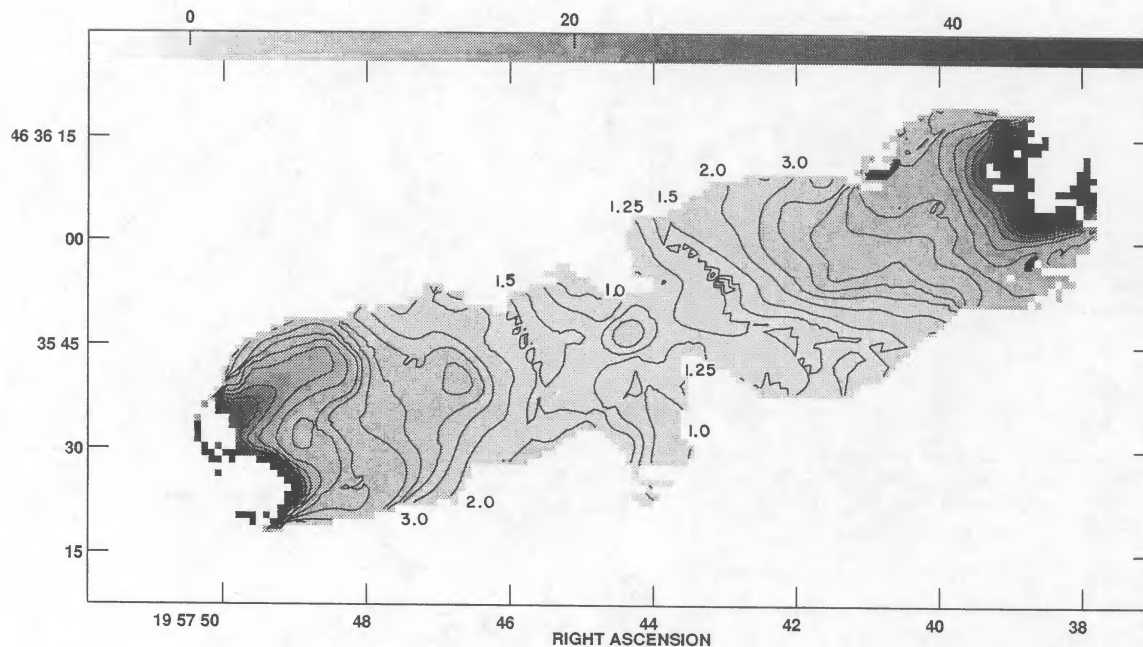


FIG. 7a

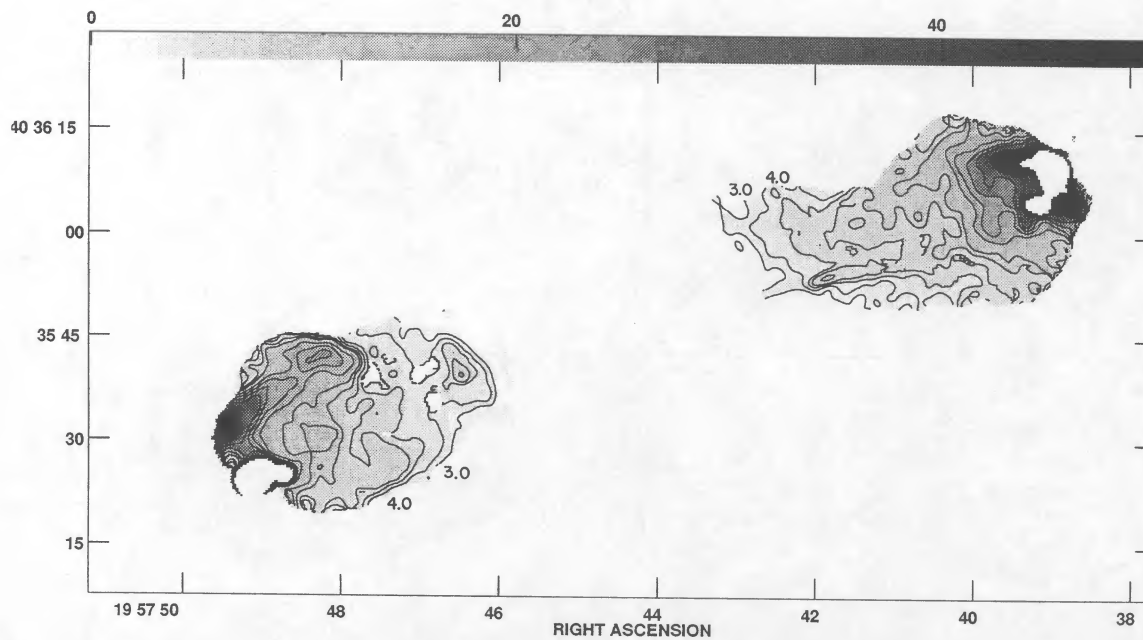


FIG. 7b

FIG. 7.—(a) Image of the break frequency distribution across the lobes of Cygnus A, as determined for the KP model spectrum fitted to data at nine frequencies between 0.15 and 22 GHz at $4''.5$ resolution, using an injection index of -0.7 . Contour levels are 1, 1.25, 1.5, 2, 3, 4, 5, 6, 8, 10, 15, 20, 25, 30, 35, and 40 GHz. Contours have been superposed on a gray scale representation of the same image. The gray scale ranges from -5.0 GHz (white) to 50 GHz (black). The results for the JP model were similar. (b) Same as (a), but for six frequencies between 1.35 and 15 GHz, at $1''.5$ resolution. Contour levels are 3, 4, 5, 6, 8, 10, 15, 20, 25, 30, 40, 50, 60, and 70 GHz. The gray scale ranges from 0 GHz (white) to 50 GHz (black). (c) Same as (b), but now the contours of break frequency are superposed on a gray scale representation of total intensity at 4995 MHz, at $1''.5$ resolution. This figure shows the northern lobe of Cygnus A. The gray scale ranges from -0.01 Jy beam $^{-1}$ (black) to 1.1 Jy beam $^{-1}$ (white). (d) Same as (c), but for the southern lobe of Cygnus A. The gray scale ranges from -0.01 Jy beam $^{-1}$ (black) to 1.1 Jy beam $^{-1}$ (white).

center of filament = $19^{\text{h}}57^{\text{m}}41^{\text{s}}.5$, $40^{\circ}36'01''$), by subtracting the surrounding lobe flux assuming a ropelike geometry for the filament. We find that the spectrum is consistent with a power law of index -1.5 between 1.5 and 15 GHz, although a curved JP or KP spectrum cannot be ruled out.

One interesting feature on the image of break frequency at $1''.5$ resolution is the high surface brightness "ridge" on

the northern edge of the southern lobe. The break frequency along the ridge falls from over 50 GHz at the eastern end of the ridge down to about 18 GHz in the middle of the ridge, and then rises again to about 25 GHz at the western end of the ridge.

Another interesting region at $1''.5$ resolution is the "spur" in the northern lobe. The spur is a linear feature which extends

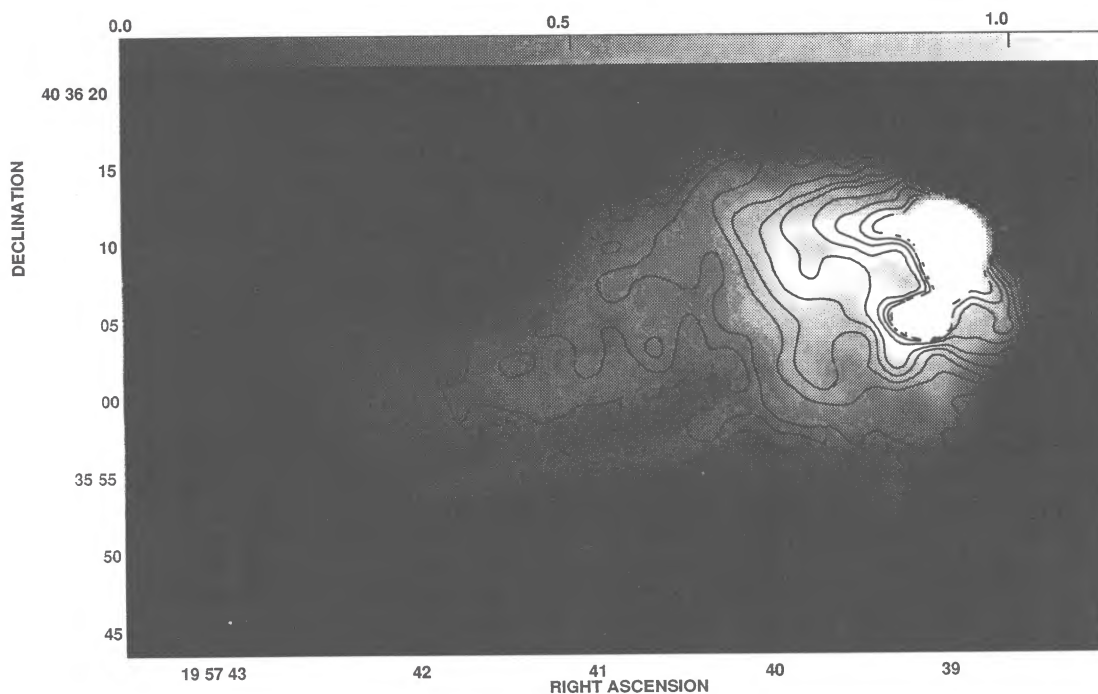


Fig. 7c

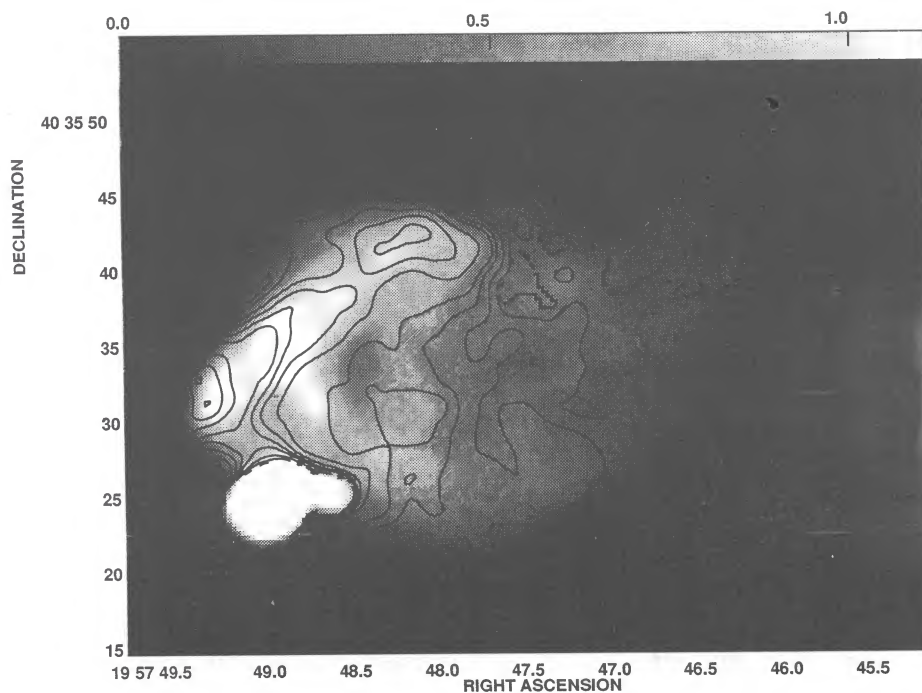


FIG. 7d

from hot spot A toward the core for a distance of about $12''$. It forms the northern edge of the brightest loop in the head of the northern lobe (center position = $19^{\text{h}}57^{\text{m}}39^{\text{s}}.5$, $40^{\circ}36'12''$). The break frequency falls from over 50 GHz near the hot spot to below 20 GHz at a distance of 12 kpc away from the hot spot. In § 5.1.2 we present arguments for collimated outflow from the hot spot along this feature.

The jet in the tail of the northern lobe is clearly visible in the image of break frequency at $1''.5$ resolution. The jet shows

higher break frequencies than its environs—higher by a factor of about 2. Again, confusion with lobe emission is a problem when analyzing the jet spectrum, especially at low frequency. We find that most of the jet knots within 25 kpc of the core (Perley et al. 1984) have spectra consistent with a power law between 1.5 and 15 GHz, with an index of -0.8 ± 0.2 . However, the data cannot rule out a curved JP or KP spectrum over this range. In between the knots, the upper limit to the spectral index of the jet between 5 and 15 GHz is -0.5 .

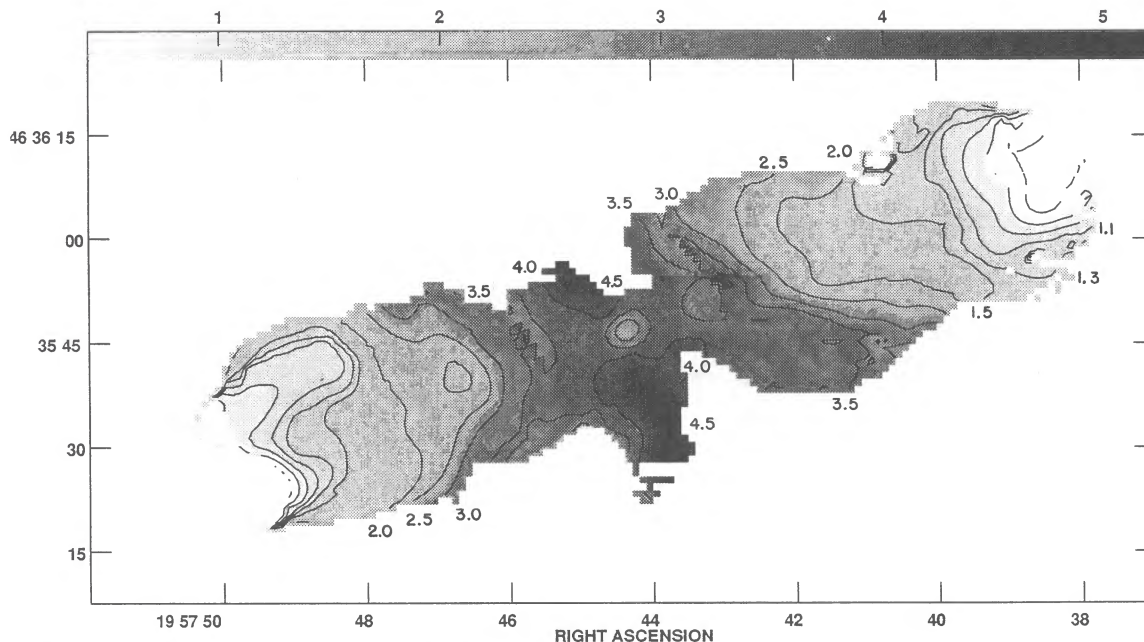


FIG. 8.—Image of spectral age, as calculated from the break frequency distribution of figure 7a, using eq. (1) and assuming a constant magnetic field strength of $50 \mu\text{G}$. Contour levels are 0.5, 0.7, 0.9, 1.1, 1.3, 1.5, 2.0, 2.5, 3.0, 3.5, 4.0, 4.5, and 5.0 Myr. The gray scale ranges from 0.4 Myr (white) to 5.2 Myr (black).

This limit also applies to the counter jet seen at 5 GHz (Dreher et al. 1987b). Since the spectral evolution along the jet is independent of that in the lobes, we leave a physical discussion of the jet spectrum to a later paper.

5. DISCUSSION

5.1. Spectral Ages and Source Dynamics

5.1.1. Lobes

Equation (1) relates the observed break frequency to the synchrotron “age” of the distribution. In Figure 8 we show the resulting distribution of spectral age, as calculated from the break frequency distribution at $4''.5$ resolution and equation (1), using a constant magnetic field strength of $50 \mu\text{G}$. The dominant morphological feature in the image of spectral age is increasing age with increasing distance from the hot spots. Such a morphology provides compelling evidence for source models in which the relativistic electrons originate in the hot spots.

The lowest break frequency in Cygnus A is 750 MHz. It occurs in the plume extending south from the center of the bridge. A break frequency of 750 MHz implies an age of the source of 6 Myr, assuming minimum-energy fields.

Figures 9a and 9b plot spectral age as a function of distance from the hot spot for the northern and southern lobes in Cygnus A, respectively, along a line extending down the center of the lobes toward the core. The error bars reflect the formal errors in the fitting results for v_B . For the magnetic field strength at each position, a weighted mean of the minimum-energy fields (weight $\propto B^{3/2}$) calculated along the line from the hot spot to the point in question was used. Such fields are valid if (1) minimum-energy conditions apply, (2) the gradient in minimum-energy fields down the lobes represents the true magnetic history of the radiating fluid, and (3) the particles have spent equal time in each region of different field strength.

The linear fits to the data imply flow velocities of $v_{\text{sep}} = 0.06c \pm 0.01c$ in the northern lobe, and $v_{\text{sep}} = 0.05c \pm 0.01c$ in the southern lobe, where v_{sep} is the “separation velocity” between the site of particle injection (at the heads of the lobes) and the waste jet material. The velocities change by only a few percent if we simply assume a constant field of $50 \mu\text{G}$, and they depend on the Hubble constant as $H_0^{-4/7}$.

The linear fits in Figure 9 do not extrapolate to zero age at zero distance. The zero-age offset is about 0.1 Myr in the northern lobe and 0.2 Myr in the southern lobe. Such an offset has been seen in other sources (Alexander 1987; Stephens 1987), and may arise from expansion losses as the fluid flows from the hot spots into the radio lobes. If this is the case, then the corresponding “starting” break frequency in the radio lobes is about 400 GHz. A simple spherical model (expansion by a factor of 2; see § 5.2.2) then predicts a cutoff in the spectrum of the hot spots at around 10^{13} Hz, which is consistent with the lower and upper limits set by Eales, Alexander, & Duncan (1989) and Kronberg, van den Bergh, & Button (1977), respectively.

Winter et al. (1980) point out that the separation velocity measured by spectral aging techniques is the sum of two velocities, namely, the advance speed of the radio lobe, v_{adv} , and the speed of the backflowing lobe material, v_{bf} , with both velocities measured in the rest frame of the associated galaxy. An important question is whether the waste hot spot material is simply left behind by the advancing lobe ($v_{\text{bf}} = 0$) or whether there is actually bulk flow back toward the galaxy? From continuity, it is easy to see that a large backflow velocity requires a large radio plume to hold the backflowing material (or some other physical sink for the relativistic particles), or substantial compression of the flow near the center of the source. In the case of Cygnus A, compression in the center of the radio bridge can be ruled out, since there is no corresponding rise in low-frequency surface brightness. Also, at 327 MHz, the observed volume of the radio plumes in Cygnus A (assuming a disklike geometry)

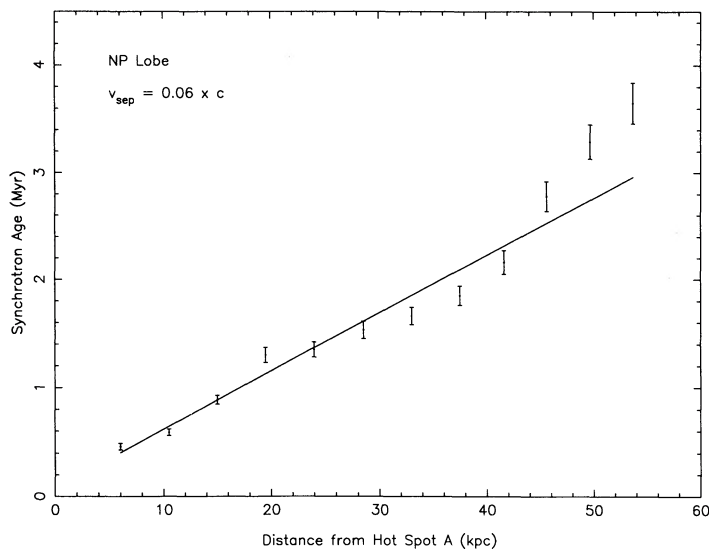


FIG. 9a

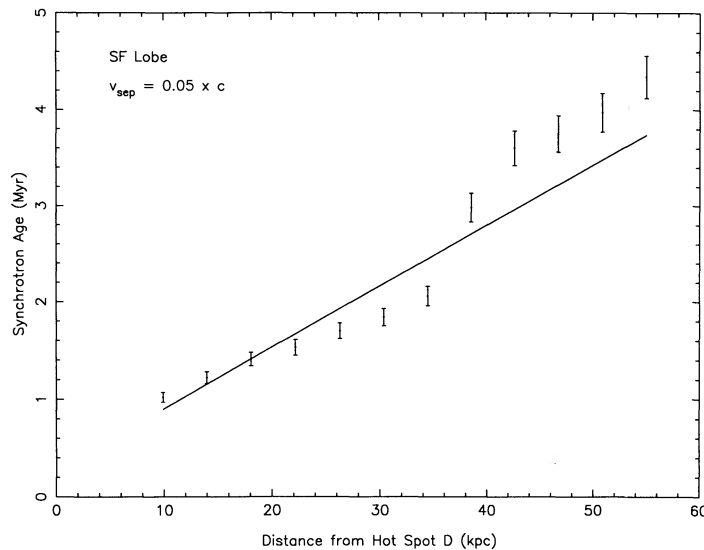


FIG. 9b

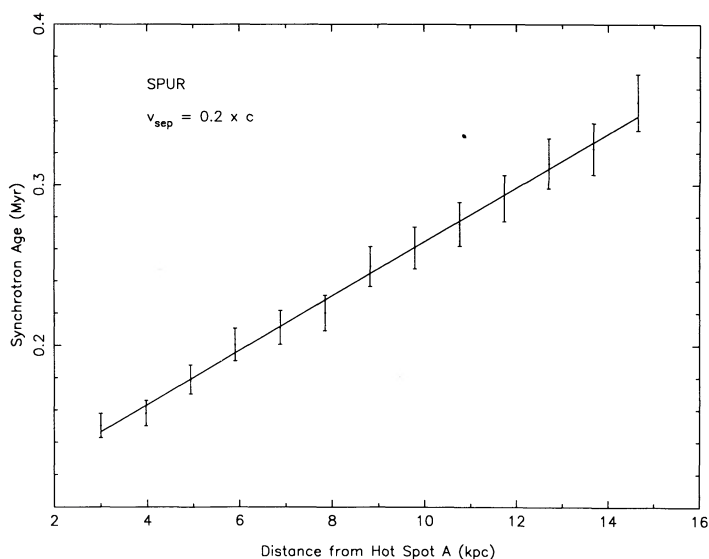


FIG. 9c

FIG. 9.—(a) Plot of spectral age vs. distance along a line running down the center of the northern lobe of Cygnus A. Ages were determined from the break frequency distribution for the KP model spectrum at $4''.5$ resolution. The fields used for the age calculation are described in the text. Zero distance equals the hot spot position. The solid line is a linear fit to the data, and implies a separation velocity of 0.06 ± 0.01 times the speed of light. (b) Same as (a), but for the southern lobe. The straight-line fit implies a separation velocity of 0.05 ± 0.01 times the speed of light. (c) Plot of age vs. distance from hot spot A along the “spur” in the northern lobe. The ages were calculated from the break frequencies on image 8B, at $1''.5$ resolution, using a field of $100 \mu\text{G}$. The straight-line fit implies an outflow velocity of 0.2 times the speed of light.

is at most about $\frac{1}{4}$ that of the radio lobes. Therefore, the backflow velocity in Cygnus A is likely to be less than about $\frac{1}{4}$ that of the advance speed, unless we can find an alternate sink for the backflowing relativistic particles.

An independent estimate of v_{adv} can be made by assuming ram-pressure confinement of the advancing lobes by the X-ray-emitting cluster gas external to the radio lobes (Arnaud et

al. 1984). For the hot spots, this leads to an advance speed of $0.02c$, assuming minimum pressures. Williams (1985) has shown that for sources in which the hot spots cover only a small fraction of the front surface of the lobe, such as Cygnus A, the overall advance speed of the source due to the pressure of the hot spot is lower than the instantaneous advance speed of the hot spot by the ratio of the area of the hot spot to the area of the front surface of the lobe. For Cygnus A this ratio is about 16, which implies a fairly slow source advance due to the averaged hot spot pressure of $0.0013c$, under minimum conditions.

If we consider the minimum pressure of the radio-emitting fluid surrounding the hot spots at the heads of the radio source, we find an advance speed of about $0.005c$ for Cygnus A. This is larger than the source advance speed due to the averaged hot spot pressure, implying that the overall advance of the source is dominated by the pressure of the regions surrounding the hot spots, and not by the hot spots themselves (assuming minimum-energy conditions). The implied Mach number for the advancing source with respect to the sound speed in the unperturbed cluster gas is about 2 (Arnaud et al. 1984).

However, we are left with the problem that the source advance speed under the assumption of ram-pressure confinement, and using minimum-energy lobe pressures, is much smaller than the measured separation velocity. This would require a large backflow velocity, and hence violates continuity arguments given above. The implications are that either (1) the pressure in the heads of the radio lobes are about two orders of magnitude larger than minimum, and hence that the true advance speed is much larger than found under minimum conditions, or (2) the magnetic fields in the lobes are smaller than minimum-energy values, and hence the separation velocity is slower than under minimum-energy assumptions, or (3) the break frequency distribution is not physically related to the true separation velocity. Note that the ram-pressure advance speed is a weak function of internal pressure ($v_{\text{adv}} \propto \text{pressure}^{1/2}$), while the separation velocity, as measured from the break frequency distribution, is a strong function of magnetic field ($v_{\text{sep}} \propto B^{3/2}$).

A possible solution is to assume that the source advance has slowed dramatically in the recent past. This could arise if, for instance, the jet has altered its direction abruptly in the recent past. Such a scenario is addressed in the simulations of Williams & Gull (1985), from which they find that the source advance speed slows by a factor of about 4 between the axisymmetric stage, when the source advance is equal to the hot spot advance, and the nonaxisymmetric stage, when the jet does most of its work widening, and not advancing, the radio lobes. However, for the case of Cygnus A, we find this model unsatisfactory for the reason that even the instantaneous hot spot advance speed is too slow to explain the discrepancy between v_{adv} and v_{sep} .

A self-consistent solution would be to assume that the fields in the radio source are about a factor of 3 lower than minimum energy. This would both raise the total pressure in the relativistic particles and fields (by a similar factor) and decrease the separation velocity by a factor of about 5. In this case, $v_{adv} \approx v_{sep} \approx 0.01c$, and the source is older than under minimum conditions by a factor of 5. For this model, the total pressure in relativistic particles and fields in the lobes of Cygnus A is about 2×10^{-10} dynes cm^{-2} , the total energy density is about 6×10^{-10} ergs cm^{-3} , and the total energy stored in the lobes is about 2×10^{60} ergs (assuming a cylindrical geometry for the lobes, with a lobe length of 60 kpc and a lobe radius of 15 kpc). For comparison, the pressure in the X-ray-emitting cluster gas enveloping the lobes is also about 2×10^{-10} dynes cm^{-2} (Arnaud et al. 1984). Hence, for the model in which the lobe magnetic field is a factor of 3 lower than the minimum-energy value, the radio bridge is roughly in pressure equilibrium with the external medium. We have no reason to reject such a moderate departure from minimum energy, nor can we rule out a source age of 30 Myr. Indeed, Feigelson et al. (1987) have measured the magnetic fields in the radio halo of M87 by comparing X-ray and radio observations, and find that the fields are lower than minimum energy by a factor of 3–8. Also, a velocity analysis, similar to the one herein, for the powerful radio galaxy 3C 295 (Perley & Taylor 1991) argues for lobe fields a factor of 3 below minimum-energy values in that source. The physical parameters derived for the two source models discussed above (i.e., the minimum-energy model and the self-consistent model) are summarized in Table 4.

The contours of v_B appear to converge toward the edges of the lobes. This morphology suggests a slower separation velocity along the edges of the lobes than down the center. The implied velocity along the edges of the lobes is $0.03c$, or roughly a factor of 2 slower than in the center. A similar morphology for v_B was found for the powerful radio galaxy 3C 20 by Stephens (1987). He suggested that this velocity gradient from the center to the edges of the lobes is due to shear flow down the radio lobes. Shear flow implies that the backflow

velocity must go to zero along the edge of the radio lobe, hence the measured separation velocity along the edge of the lobe equals the source advance speed. We reject this scenario for Cygnus A, since it would imply that about half the maximum separation velocity, as measured down the center of the lobe, is due to backflow and half is due to source advance, and, again, such a large backflow velocity is inconsistent with continuity.

A more reasonable interpretation of the age gradient from the center to the edges of the lobes in Cygnus A is to assume that the magnetic fields are higher along the edges of the lobes than in the center, and hence that aging occurs more rapidly along the edges. The required increase in fields from center to edge is about 60%. One would then expect a modest edge brightening of the lobes. The “square” brightness profile of the diffuse emission in the radio lobes (Carilli 1989) is consistent with this scenario.

Spangler (1979) has raised the question of whether the observed spectral aging in the radio lobes measures the bulk flow velocity or the relativistic electron diffusion velocity. Even if the particles stream at near the speed of light, tangling of the field lines will make diffusion a rather slow process. Considering a simple random walk in a tangled field, particle diffusion from the heads to the bridge can be ignored as long as the field is tangled on scales less than $(v_{sep}/c)L$, where v_{sep} is the measured transport velocity, L is the length of the radio lobe, and c is the maximum streaming velocity (the speed of light). In the case of Cygnus A, this limit is about 4 kpc (assuming minimum-energy fields), which is larger than the size scale of field curvature observed in the lobes of Cygnus A (Dreher et al. 1987a). Note that this limit is very conservative, since the average streaming velocity for the particles is likely to be considerably less than the speed of light. Hence, diffusion is probably not an important global transport process in the lobes of Cygnus A, although it may still be important on scales less than a few kiloparsecs.

5.1.2. Hot Spots

It has long been known that each lobe of Cygnus A contains two hot spots situated at the ends of the lobes (Hargrave & Ryle 1974; Carilli et al. 1989a). The nature of double hot spots in radio galaxies, and in particular the primary-secondary model for double hot spots, has been discussed in detail in a number of places (Williams & Gull 1985; Carilli et al. 1988; Carilli et al. 1989a; Eales et al. 1989). In this paper we restrict our analysis to the spectra of the “secondary” hot spots in Cygnus A. The large secondary hot spots located at the edge of each radio lobe contain the majority of the total energy in the hot spots in Cygnus A, and their morphology resembles, roughly, that expected for a terminal Mach disk in a hypersonic jet (Norman et al. 1982; Carilli et al. 1989a). The compact

TABLE 4
TWO SOURCE MODELS

Model	Magnetic Field (μG)	Pressure ^a (dynes cm^{-2})	Energy Density ^a (ergs cm^{-3})	Total Energy ^a (ergs)	v_{sep} ^b	v_{adv}	v_{bf}	Source Age (Myr)
Minimum-energy	50	8×10^{-11}	2×10^{-10}	8×10^{59}	0.05	0.005	0.045	6
Self-consistent	17	2×10^{-10}	6×10^{-10}	2×10^{60}	0.01	0.01	0	30

^a Pressure, energy density, and total energy are the sum of those in relativistic particles and magnetic fields.

^b Velocities are in units of the speed of light.

“primary” hot spot in each lobe is recessed from the lobe extremity, and hence the spectra for the primaries are confused by emission from the lobes, especially at 4'' resolution. We leave a detailed discussion of the spectrum and role of the primaries to a future paper, pending observations at higher frequencies and spatial resolutions.

The break frequency in hot spot A implies a synchrotron age of 1.2×10^5 yr, while that in hot spot D implies an age of 9.0×10^4 yr, using minimum-energy fields. These ages can be interpreted according to the dynamical model for hot spots given in § 2. The implied outflow velocity in hot spot A is $0.07c$, while that in hot spot D is $0.09c$, where we have assumed an outflow distance equal to the HWHM of the beam, or 2.5 kpc.

Given the high temperatures and low densities expected in jets and hot spots in radio galaxies, it is reasonable to assume that the terminal jet shocks are nonradiative. For a strong, nonradiative shock, the inflow velocity is 4 times the outflow velocity. Under this assumption, the inflow velocities, v_{in} , for the secondary hot spots in Cygnus A are $v_{in} \approx 0.3c$. A similar analysis of hot spots in three other radio galaxies by Meisenheimer et al. (1989) found inflow velocities ranging from 0.16c to 0.51c.

According to the simple, axisymmetric outflow model of Meisenheimer et al. (1989), the particle distribution should be segregated according to age and distance from the shock. The model then predicts that, at high spatial resolution, one should see at the edge of the hot spot (i.e., 2'' from the shock) a JP or KP spectrum, depending on the efficiency of pitch-angle scattering with a spectral break around 10 GHz. Our observations at 1'' resolution are adequate to look for such behavior in the break frequency distribution in the vicinity of the hot spots in Cygnus A. For hot spot D in the southern lobe, there is a very sharp gradient in break frequency going from the hot spot to the lobes, where the break frequencies fall quickly to below 15 GHz. This is consistent with the simple outflow model above. But for hot spot A, break frequencies as high as 70 GHz are found about 2'' from the center of the hot spots, and the gradients in break frequency vary considerably with position around the hot spot.

The fact that break frequencies much larger than 10 GHz are observed beyond a few arcseconds from the hot spot is clearly inconsistent with the simple hot spot model of Meisenheimer et al., involving particle injection at a single point (i.e., the terminal jet shock) and radiative losses in an axisymmetric outflow from this point. There are a number of effects which could lead to such a break frequency morphology in the hot spot vicinity. First, there is the possibility of spatially distributed particle acceleration. Second, there is the possibility that the postshock flow pattern is very complex and asymmetric, with some parcels of fluid flowing quickly away from the shock and others leaving the hot spot more slowly. Last, there is the possibility of rapid relativistic particle diffusion on scales of a few kiloparsecs or less (see § 5.1.1). Any of these effects, or a combination of them, would result in regions along the edges of the hot spots with break frequencies considerably larger than those predicted from the hot spot spectra at low resolution, and could lead to a mixing of the electron populations with different ages as they flow away from the shocks. If this is the case, then the hot spot break frequency calculated from observations at 4'' resolution measures (roughly) an intensity-weighted mean outflow velocity, and the simple relationship between this velocity and the inflow velocity given above is no longer valid.

Considering the possibility of spatially distributed particle

acceleration, the extended optical synchrotron emission around the hot spots in the powerful radio galaxy Pictor A provides strong evidence for spatially distributed particle acceleration in the vicinity of the hot spots in at least one source (Meisenheimer et al. 1989). A possible mechanism for accelerating particles in the turbulent outflow from the terminal jet shock is stochastic (second-order) Fermi acceleration (cf. Longair 1981).

Considering the possibility of complex postshock flow patterns, asymmetric and turbulent outflow from the hot spots is consistent with the complex morphology of the high surface brightness structures seen on images of the Cygnus A hot spots at high resolution (Carilli et al. 1989a).

Relevant to this latter argument is the observed distribution of break frequency along the “spur” discussed in § 4.3.2. The morphology of this feature suggests collimated outflow from the hot spot. The outflow scenario is supported by the distribution of v_B , which shows a clear decrease in v_B with distance from the hot spot. In Figure 9c we show a linear fit of distance versus age along this feature. If we use the minimum-energy field of 100 μ G (derived assuming a ropelike geometry for the feature), we find an outflow velocity of $0.2c$. This is considerably larger than the “mean” value from the analysis of the integrated hot spot spectrum at 4'' resolution, and hence is consistent with the idea of asymmetric outflow from the hot spots. For comparison, the gradient in the break frequency distribution with distance from the hot spot along a line parallel to the spur, but 5'' to the south of it, implies an outflow velocity of $0.07c$ (again, using minimum-energy fields).

Overall, there is strong evidence that the simple axisymmetric outflow model for hot spots given by Meisenheimer et al. (1989) may be too simple, and that effects such as highly asymmetric outflow and spatially distributed particle acceleration in the hot spot vicinity may be important. High-resolution observations at high frequency (better than 0'' resolution at frequencies above 50 GHz) are required to clarify the spectral behavior on the complex, high surface brightness structures in the vicinity of the hot spots of Cygnus A, and in particular to study the role of double hot spots in the generation of relativistic particles in radio galaxies.

5.2. Spectral Shape

5.2.1. High-Frequency Steepening

One important result from our analysis of the high-frequency behavior of the source spectra is the clear distinction between the hot spots and the lobes. The hot spot spectra steepen much more gradually at high frequency than the lobe spectra, and are well described by the continuous injection model. The spectra of emission from the radio lobes show much greater steepening than allowed by continuous injection. Hence, we have further support for models in which particles are accelerated at the hot spots, and subsequently lose energy in the radio lobes.

An important result for the lobe spectra is that the high-frequency steepening is less than exponential. The lobe spectra are reasonably fitted by the KP model spectrum. The most straightforward explanation for this is to assume no pitch-angle scattering in the radio lobes. However, such a conclusion conflicts with theories concerning cosmic-ray propagation, and in particular with the study of cosmic rays in the disk of our own galaxy. Galactic cosmic rays are thought to be isotropized very quickly (in a frame traveling at the Alfvén speed), owing to scattering by self-induced Alfvén waves (cf. Wentzel 1969,

1974). A possible way to avoid such scattering is to damp these waves. However, physical conditions in the radio source (high temperatures, low densities) suggest that wave damping should not be important. A second possible way to maintain an anisotropy in the pitch-angle distribution is for the Alfvén speed to approach the speed of light (Longair 1981). For Cygnus A this would occur if thermal densities in the lobe are very low, i.e., less than 10^{-7} cm^{-3} using minimum-energy fields. Such a low density cannot be ruled out by present, model-dependent upper limits to the thermal particle densities in the lobes of Cygnus A (Dreher et al. 1987a). An important point to keep in mind is that pitch-angle scattering of the up-streaming particles at the terminal jet shock is a requirement of first-order Fermi acceleration (Bell 1978a, b; see § 5.4). If we accept the idea that there is no pitch-angle scattering in the lobes, then we must make the ad hoc assumption that the efficiency of pitch-angle scattering is much higher in the jet than in the lobes, or we must find another mechanism to stop the up-streaming particles at the terminal jet shock.

There is also the possibility of a physical mixing of the particle distributions of different ages. Possible causes for such a mixing could be a turbulent backflow or local diffusion of relativistic particles. In this case, the spectral break would be smoothed out in a way similar to that discussed for beam smearing in § 4.3.2. If this is so, then the spectral models would require another free parameter, namely, the relative age-density distribution for a given parcel of synchrotron-emitting fluid.

5.2.2. Injection Index

5.2.2.1. Fermi Acceleration

For first-order Fermi acceleration at a strong shock in the diffusive outflow limit, the power-law injection spectral index obeys the formula: $\alpha_{\text{in}} = 3/(2 - 2r)$, where r is the shock compression ratio (Bell 1978a, b; Blandford & Ostriker 1978). For a strong, nonrelativistic shock in a Newtonian fluid, $r = 4$, and hence $\alpha_{\text{in}} = -0.5$. However, a number of authors have shown that this simple relationship between α_{in} and r breaks down when considering either relativistic shocks or shocks in which the fields and relativistic particles alter the shock dynamics (Heavens 1989; Kirk & Schneider 1987; Drury & Volk 1981; Axford, Leer, & McKenzie 1982). Models including some of these effects lead to spectral indices ranging from -0.35 to -0.63 .

The injection index for both hot spots in Cygnus A is -0.5 . A similar result was found by Meisenheimer et al. (1989) for hot spots in three other powerful radio galaxies. This suggests that the terminal jet shocks in powerful radio galaxies are strong and nonrelativistic, and are dominated by thermal plasma.

It has also been suggested recently that Fermi acceleration may not be required in hot spots, and that either simple adiabatic compression of the jet (Mathews 1989) or "shock drift" acceleration (Begelman & Kirk 1990) plays the dominant role. Considering adiabatic compression, Scheuer (1989) has shown that the surface brightness going from the jet to the hot spot will change by at most a factor of 40, for a spectral index of -0.5 . For Cygnus A, a lower limit to this change at 15 GHz, $0''.1$ resolution is 100 (Carilli et al. 1989a), so we can rule out simple adiabatic compression as the sole cause for the increase in surface brightness at the hot spots. Considering shock-drift acceleration, a requirement of this mechanism (as with adiabatic compression) is the preservation of the spectral index of

the jet. Hence, if one can show that the jet spectrum is power-law over a broad range in frequency, and that the power-law index changes going from the jet to the hot spots, this model can be ruled out. In Cygnus A the jet knots show spectral indices of -0.8 between 1.5 and 15 GHz, while the hot spots have spectral indices of -0.5 . This change in spectral index argues against shock-drift acceleration as the sole cause of the brightness enhancement going from the jet to the hot spots. Of course, we cannot rule out the possibility of a curved jet spectrum, with a flatter spectral index at frequencies below those observed. Perhaps a more telling argument against shock-drift acceleration is that it occurs only in oblique shocks, which is probably not the case for the secondary hot spots, A and D, in Cygnus A (Carilli et al. 1988).

5.2.2.2. The Injection Index Discrepancy

The injection index for the radio lobes was found to be fairly uniform across the source, with a value of -0.7 . The uniformity of α_{in} across the source suggests that the injection index has not varied over time. However, a value of -0.7 is not consistent with the hot spot injection model, for which the injection index in the lobes should equal either the high-frequency spectral index in the hot spots (-1.0), if expansion losses going from the hot spot to the lobe are large, or the hot spot injection index (-0.5), if expansion losses are small. A similar discrepancy between the observed lobe injection index and that expected for hot spot outflow models was found for a number of the sources in the studies of Stephens (1987).

One possible solution to this discrepancy is to assume energy-dependent particle diffusion in the radio lobes. This explanation is often invoked for cosmic rays in spiral galaxies, for which the spectral index of radio emission changes going from the injection sites (i.e., supernova remnants) to the disk (Lerche & Schlickeiser 1982a, b). We feel this explanation unlikely for radio galaxies, since diffusion is probably insignificant compared with convection for relativistic electron transport in the lobes (see § 5.1.1).

Another possible solution to the injection index discrepancy is to assume intermediate expansion losses, i.e., that the low-frequency portions of the lobe spectra sample the part of the hot spot spectrum with slope -0.7 . Implicit in this solution is the assumption that the energy spectrum injected into the lobes is that dictated by the CI model, and hence that mixing of the various age populations in the outflow from the shocks is efficient (i.e., that the populations are not segregated by distance from the shock; see § 5.1.2).

We have tested this solution by scaling the best-fit hot spot model spectrum to fit the low-frequency data of a spectrum of the radio lobe taken at a position $9''$ back from the hot spot (see curves 1 and 2 in Fig. 5). The scaling was done in both frequency and emissivity, as expected for adiabatic expansion losses, but no assumptions were made as to the nature of the scaling law, since this depends on the geometry of both the expansion and the magnetic fields. For both lobes in Cygnus A, we find that a reasonable fit can be found. The reason this is so is that the curvature of the CI model is extremely gradual, occurring over about two orders of magnitude in frequency (see Fig. 1).

The hot-spot-to-lobe scaling law for the Np lobe is consistent with spherical expansion and an isotropic magnetic field (Scheuer & Williams 1968), with a linear scaling factor ≈ 2 . The hot-spot-to-lobe scaling law for the Sf lobe implies a large scaling in frequency, with little scaling in emissivity. This is not

consistent with a simple spherical expansion from the hot spot to the lobes. If we force the scaling law in the Sf lobe to be consistent with a spherical expansion model, the value of χ^2 increases by an order of magnitude. We conclude that a reasonable hot-spot-to-lobe spectral scaling law can be made in both lobes, but that the physical interpretations of the results are ambiguous.

One consequence of the intermediate expansion loss model is that a proper aging analysis in the radio lobes would begin with a (possibly curved) hot spot spectrum scaled in frequency and emissivity by the appropriate factors (Leahy 1990). In practice, such a process would be very difficult, both because one would have to determine the proper scaling laws empirically, which is a very uncertain process, and because the algorithms to generate aged spectra would then become much more complex. In our analysis of § 4.3.2, we have approximated this process by fitting for the low-frequency spectral index in the lobes. We should point out that for a curved injection spectrum, a spectral aging analysis will be valid only if the “injected” curvature over the observed frequency range is much less than that induced by aging. Otherwise, the break frequency determined under the assumption of power-law injection will lead to an overestimate of the true age of the particle distribution.

A conclusive test of intermediate expansion losses would be to observe at frequencies below 151 MHz with the same resolution as existing observations. The expectation is that the lobe spectra should flatten to a power law of index -0.5 at very low frequency. If such a flattening is not observed, then we must assume that the particle energy distribution is changed on leaving the hot spots through spatially extended particle acceleration.

We conclude that the injection index discrepancy between the hot spots and the lobes is an important, unsolved mystery. This is especially true in light of the similarity of the problem in many sources. This discrepancy may have important implications for physical models of relativistic particle generation in powerful radio galaxies.

5.3. *In Situ Particle Acceleration in the Radio Lobes?*

Much attention has been paid to the possibility of in situ particle acceleration in radio lobes (cf. Alexander 1987; Wiita & Gopal-Krishna 1990). A discussion of the possibility of spatially extended particle acceleration in the vicinity of the hot spots is given in § 5.1.2. In this section we discuss other regions outside of the hot spots where in situ particle acceleration may be occurring.

In situ particle acceleration in radio lobes could raise the high-frequency spectra distribution as well as redistribute electrons at low energies, and hence might explain both the lack of a high-frequency cutoff (§ 5.2.1) and the discrepancy in hot spot and lobe injection indices (§ 5.2.2) found for Cygnus A. Reacceleration mechanisms discussed for radio lobes include stochastic processes in turbulent plasmas (Longair 1981; Kardashev 1962) and resistive reconnection of ambient magnetic fields (Eilek 1982; Biskamp 1989; Christiansen 1989). The facts that we see spectral aging down the lobes and that the spectra steepen according to the KP model suggest that particle acceleration is not a dominant process in the radio lobes.

Could the filamentary structures in the lobes of Cygnus A be related to in situ particle acceleration? Higher break frequencies on the filaments may signal localized particle acceleration, as might be expected if the filaments were weak shock

fronts propagating through the lobes. This scenario is supported by the lack of spectral evolution along the length of the most prominent filament in the northern lobe (Fig. 7c). However, such a morphology could also arise from simple compression of the fluid, as might be expected if the filaments were nonlinear (Mach 1) sound waves.

Another region with very interesting spectral structure, suggestive of local particle acceleration, is the bright ridge in the southern lobe. In § 4.3 we found that break frequencies rise with increasing distance from the hot spot along this feature. This rise in break frequency is not due to compression of the fluid as it approaches the western end of the ridge, since the low-frequency surface brightness remains fairly constant across the feature. The peak break frequency at the eastern end of the ridge is about 50 GHz. One possible scenario for the spectral morphology along this feature is that the eastern end of the ridge represents the position of an “old” hot spot, no longer being supplied by the jet, and that there is supersonic backflow along the ridge away from this dead hot spot, which shocks at the far end of the ridge, accelerating new particles. This scenario implies a time scale for changes in jet direction (i.e., hot spot position) of about 2×10^5 yr. Conversely, we could assume that the fluid at the two ends of this feature has different origins. In this case, a study of the spectral evolution from one end of the feature to the other is meaningless.

5.4. *A Low-Energy Cutoff and Shock Acceleration Theory*

We have found in § 4.2 that the spectra of the hot spots flatten from the injection power law at low frequency. One possible explanation for the low-frequency flattening in the hot spots is synchrotron self-absorption (SSA). Fitting a self-absorbed spectrum results in $\nu_1 = 165 \pm 10$ MHz in both hot spots, where ν_1 is the frequency at which the synchrotron optical depth equals 1 (Figs. 4c and 4d and Table 3). However, the sharp inversion required by synchrotron self-absorption is poorly fitted by the gradual flattening seen in the hot spot spectra. A possible solution to the poor fit is to allow for a large range in ν_1 within the 4"5 beam, as might be expected given the wealth of structure in the hot spots seen at higher resolution (Carilli et al. 1989a). The real problem with synchrotron self-absorption is that the implied magnetic field strength in the self-absorbed region is 3 G, which is four orders of magnitude larger than fields derived from minimum-energy arguments. We feel that such a large departure from minimum conditions is highly unlikely, since it implies pressures eight orders of magnitude larger than minimum, and synchrotron aging times in the hot spots lower by six orders of magnitude.

Another possible explanation for the low-frequency flattening is thermal absorption. We can rule out internal thermal material, since the required particle densities (≥ 2 cm $^{-3}$ for a 10^4 K gas) would Faraday depolarize the radio emission. For the same reason we reject the Razin-Tsytoich effect. We can rule out Galactic thermal material, since the phenomenon is isolated to the hot spots. We can rule out cluster gas, since we see no optical H α emission from the hot spot regions (Carilli et al. 1989b).

The most likely explanation for the low-energy flattening of the hot spot spectra is a low-energy cutoff (LEC) in the relativistic particle distribution. Fitting such a spectrum results in a reasonable fit (see Fig. 4 and Table 3), with $\nu_{co} = 190 \pm 20$ MHz in hot spot A, and $\nu_{co} = 220 \pm 20$ MHz in hot spot D, where ν_{co} is the cutoff frequency defined in equation (6.33) of

Pacholczyk (1970). Using minimum-energy fields then leads to a cutoff Lorentz factor of $\gamma_{\text{co}} = 420 \pm 20$ for hot spot A and $\gamma_{\text{co}} = 440 \pm 20$ for hot spot D.

A low-energy cutoff in the particle distribution was first predicted in the original work on diffusive shock acceleration by Bell (1978a, b). Bell hypothesized that, in order for a particle to be “injected into the acceleration process,” it must have sufficient momentum to pass unperturbed through the potentials in the collisionless shock which act to stop the incoming jet—i.e., the relativistic electrons must see the shock solely as a velocity discontinuity. An equivalent way to view this is by considering the fact that the relativistic electrons being accelerated must have gyroradii much larger than the shock width, and that the width of a collisionless shock is of the order of the gyroradius of thermal protons in the incoming flow.

The low-energy cutoff for accelerating particles in the diffusive shock acceleration mechanism is often called “the injection problem” (Eilek & Hughes 1990). The calculation of Eilek & Hughes shows that the threshold for electron Lorentz factors, γ_{co} , occurs at $\gamma_{\text{co}} = 2\gamma_{\text{in}}(v_{\text{in}}/c)(m_p/m_e)$, where γ_{in} is the Lorentz factor for the incoming flow and v_{in} is the inflow velocity. Using the value of γ_{co} derived assuming minimum-energy fields above, we find an inflow velocity of $0.12c$ for the hot spots in Cygnus A. This is somewhat lower than the inflow velocity measured from the hot spot break frequency in § 5.1.2. The two can be reconciled by lowering the hot spot field by 30% from minimum energy, with the self-consistent hot spot field being about $200 \mu\text{G}$, and the inflow velocity is then $0.2c$.

A second mechanism which could lead to a low-energy flattening in the electron energy spectrum is damping by charge separation of the Alfvén waves which resonate with the low-energy portion of the relativistic electron distribution. Alfvén waves are required to stop the up-streaming relativistic particles and hence allow them to be reconnected across the super-Alfvénic shock. Eilek & Hughes (1990) have considered this effect, and find a low-energy cutoff at $\gamma_{\text{co}} = (m_p v_A/m_e v_{\text{in}})$, where v_A is the preshock Alfvén speed. Comparing the cutoff set by wave damping with that set through momentum arguments above, we find that wave damping dominates in relativistic jets. If this applies in the hot spots of Cygnus A, then the Alfvén Mach number of the incoming flow is 4.3 (using minimum-energy fields).

6. SUMMARY

The results from our extensive spectral study of the radio emission from the powerful radio galaxy Cygnus A are in good agreement with the jet model for powerful radio galaxies. In this model, energetic particles are generated at the terminal jet shocks (i.e., the radio hot spots), and then expand into the radio lobes, subsequently losing energy through synchrotron radiation.

Because of the unprecedented frequency coverage of these observations, we were also able to validate the theoretical picture of the synchrotron aging process, which had been widely used but never thoroughly tested before. Somewhat to our surprise, the JP aging model, which makes the physically plausible assumption that the electron pitch-angle distribution is kept isotropic by scattering processes, does not fit our data for the lobes. The KP model, without pitch-angle scattering, does fit quite well, however.

The data for the hot spots are well fitted by the continuous

injection model spectrum. We find an injection index of -0.5 for both hot spots. This is consistent with diffusive shock acceleration at a strong, nonrelativistic shock in a Newtonian fluid, although it does not preclude other models. Both hot spots have spectral break frequencies around 10 GHz. Above the break, the hot spot spectra remain power-law with index -1.0 out to at least 375 MHz. The low-frequency hot spot emission spectrum falls below the injected power law. This effect is isolated to the hot spots, and is best explained by a low-energy cutoff in the particle distribution, as predicted by Bell in his original work on diffusive shock acceleration.

We find that expansion losses are large going from the hot spots to the lobes, but that in the lobes themselves the dominant energy loss mechanism is synchrotron radiation. The break frequency distribution across the lobes at $4''.5$ resolution shows a clear trend of increasing break frequency with distance from the hot spot, which supports dynamical models for powerful radio galaxies in which the energetic particles are injected into the lobes by the hot spots. The lowest break frequency in the source is 750 MHz, which corresponds to a source age of 6 Myr in minimum-energy magnetic fields. The separation velocity assuming minimum-energy fields is $0.06c$. This is much larger than the source advance speed required for ram-pressure confinement of the heads of the lobes, assuming minimum pressure configuration for the particles and fields. A self-consistent model is possible in which the fields are a factor of 3 below minimum-energy values, the source advance speed is approximately equal to the separation velocity, $\approx 0.01c$, and the source age is 30 Myr. In this model, the radio “bridge” is roughly in pressure equilibrium with the external X-ray-emitting cluster gas.

At $1''.5$ resolution we find a number of interesting features in the break frequency distribution. First, the filaments in the lobes have higher break frequencies than their environs, by about 20%. Second, the “ridge” in the northern part of the southern lobe shows a rise in break frequency with distance from the hot spot. Higher break frequencies in the filaments and at the end of the “ridge” may indicate in situ particle acceleration in these features. Third, we find a clear trend of decreasing break frequency along the “spur” extending back toward the core from hot spot A in the northern lobe. This morphology suggests collimated outflow from the hot spot along this feature. Last, we find break frequencies much greater than 10 GHz beyond $2''$ from the hot spots. This is inconsistent with the hot spot break frequencies derived from observations at $4''.5$ resolution and a simple hot spot model involving particle injection at a single point (i.e., the terminal jet shock) and radiative losses in an axisymmetric outflow from this point, and suggests spatially distributed particle acceleration in the vicinity of the hot spots and/or highly asymmetric outflow.

We find a clear difference between the high-frequency behavior of hot spot spectra and that of the lobes. The hot spot spectra steepen much more gradually at high frequency than the lobes, and are well described by the continuous injection model. The spectra of emission from the radio lobes show much greater steepening than is allowed by continuous injection. Hence, we have further support for models in which particles are accelerated at the hot spots and subsequently lose energy in the radio lobes. However, we also find that the injection index for both lobes is -0.7 . Such a value is difficult to reconcile with the observed hot spot injection indices of -0.5 . The cause for this injection index discrepancy remains a mystery.

J. W. D. would like to acknowledge support from NSF grant AST 87-03525. The National Radio Astronomy Observatory is operated by Associated Universities, Inc., under cooperative agreement with the National Science Foundation. C. L. C.

would like to thank the referee, Roger Linfield, and L. Rudnick and M. Birkinshaw for useful suggestions on the paper, and T. Muxlow for supplying a digital version of his image of Cygnus A at 151 MHz.

REFERENCES

- Alexander, P. 1985, *MNRAS*, 213, 743
 ———. 1987, *MNRAS*, 225, 27
 Alexander, P., Brown, M. T., & Scott, P. F. 1984, *MNRAS*, 209, 851
 Alexander, P., & Leahy, J. P. 1987, *MNRAS*, 225, 1
 Anantharamiah, K. 1988, in *Synthesis Imaging Workshop*, ed. R. A. Perley, F. Schwab, & A. Bride (Charlottesville: NRAO), 415
 Arnaud, K. A., Fabian, A. C., Eales, S. A., Jones, C., & Forman, W. 1984, *MNRAS*, 211, 981
 Axford, W. I., Leer, E., & McKenzie, J. F. 1982, *A&A*, 111, 317
 Baars, J. M., Genzel, R., Pauliny-Toth, I. I., & Witzel, A. 1977, *A&A*, 61, 99
 Begelman, M. C., & Kirk, J. G. 1990, *ApJ*, 353, 66
 Bell, A. R. 1978a, *MNRAS*, 182, 147
 ———. 1978b, *MNRAS*, 182, 443
 Biskamp, D. 1989, in *Radio Hot Spots in Extragalactic Radio Sources*, ed. K. Meisenheimer & H.-J. Röser (Heidelberg: Springer-Verlag), 279
 Blandford, R. D., & Ostriker, J. P. 1978, *ApJ*, 221, L29
 Blandford, R. D., & Rees, M. J. 1974, *MNRAS*, 165, 395
 Bridle, A. H., & Perley, R. A. 1984, *ARA&A*, 22, 319
 Burch, S. F. 1979, *MNRAS*, 186, 519
 Carilli, C. L. 1989, Ph.D. thesis, Massachusetts Institute of Technology
 Carilli, C. L., Dreher, J. W., & Perley, R. A. 1989a, in *Radio Hot Spots in Extragalactic Radio Sources*, ed. K. Meisenheimer & H.-J. Röser (Heidelberg: Springer-Verlag), 51
 Carilli, C. L., Dreher, J. W., Perley, R. A., & Conner, S. 1989b, *AJ*, 98, 513
 Carilli, C. L., Perley, R. A., & Dreher, J. W. 1988, *ApJ*, 334, L73
 Christiansen, W. A. 1989, in *Radio Hot Spots in Extragalactic Radio Sources*, ed. K. Meisenheimer & H.-J. Röser (Heidelberg: Springer-Verlag), 291
 Clark, B. G. 1980, *A&A*, 89, 377
 Cornwell, T. J., & Evans, K. F. 1985, *A&A*, 143, 77
 Dreher, J. W., Carilli, C. L., & Perley, R. A. 1987a, *ApJ*, 316, 611
 ———. 1987b, *BAAS*, 19, 731
 Drury, L. O'C., & Volk, H. J. 1981, *ApJ*, 248, 344
 Eales, S. A., Duncan, W. D., & Alexander, P. 1989, *MNRAS*, 240, 817
 Eilek, J. A. 1982, *ApJ*, 254, 472
 Eilek, J. A., & Hughes, P. 1990, in *Astrophysical Jets*, ed. P. Hughes (Cambridge: Cambridge Univ. Press), 428
 Fanaroff, B. L., & Riley, J. M. 1974, *MNRAS*, 167, 31P
 Feigelson, E. D., Wood, P. A. D., Schreier, E. J., Harris, D. E., & Reid, M. J. 1987, *ApJ*, 312, 101
 Fogarty, W., Epstein, E., Montgomery, J., & Dworetzky, M. 1971, *AJ*, 76, 537
 Fomalont, E. B., Ebnetter, K. A., van Breugel, W. J., & Ekers, R. D. 1989, *ApJ*, 346, L17
 Hargrave, P. J., & Ryle, M. J. 1974, *MNRAS*, 166, 305
 Heavens, A. 1989, in *Radio Hot Spots in Extragalactic Radio Sources*, ed. K. Meisenheimer & H.-J. Röser (Heidelberg: Springer-Verlag), 247
 Heavens, A. F., & Meisenheimer, K. 1987, *MNRAS*, 225, 335
 Hines, D., Owen, F., & Eilek, J. 1990, *ApJ*, 347, 713
 Hobbs, R. W., Maran, S., Kafatos, M., & Brown, L. 1978, *ApJ*, 220, L77
 Jaffe, W. J., & Perola, G. C. 1973, *A&A*, 26, 423
 Kardashev, N. S. 1962, *Soviet Astron.—AJ*, 6, 317
 Kirk, J. G., & Schneider, P. 1987, *ApJ*, 315, 425
 Kronberg, P., van den Bergh, S., & Button, S. 1977, *AJ*, 82, 315
 Leahy, J. P. 1990, in *Astrophysical Jets*, ed. P. Hughes (Cambridge: Cambridge Univ. Press), 100
 Leahy, J. P., Muxlow, T. W., & Stephens, P. W. 1989, *MNRAS*, 239, 401
 Leahy, J. P., & Williams, A. 1984, *MNRAS*, 210, 929
 Lerche, I., & Schlickeiser, R. 1982a, *A&A*, 107, 148
 ———. 1982b, *MNRAS*, 201, 1041
 Longair, M. S. 1981, *High Energy Astrophysics* (Cambridge: Cambridge Univ. Press)
 Mathews, A. 1989, in *Radio Hot Spots in Extragalactic Radio sources*, ed. K. Meisenheimer & H.-J. Röser (Heidelberg: Springer-Verlag), 219
 Meisenheimer, K., Röser, H.-J., Hiltner, P., Yates, M., Longair, M., Chini, R., & Perley, R. 1989, *A&A*, 219, 63
 Meyer, S. L. 1975, *Data Analysis for Scientists and Engineers* (New York: Wiley)
 Miley, G. 1980, *ARA&A*, 18, 165
 Myers, S. T., & Spangler, S. R. 1985, *ApJ*, 291, 52
 Norman, M. L., Smarr, L., Winkler, K.-H. A., & Smith, M. D. 1982, *A&A*, 113, 285
 Pacholczyk, A. G. 1970, *Radio Astrophysics* (San Francisco: Freeman)
 ———. 1977, *Radio Galaxies* (New York: Pergamon)
 Perley, R. A. 1988, in *Synthesis Imaging Workshop*, ed. R. A. Perley, F. Schwab, & A. Bridel (Charlottesville: NRAO), 287
 Perley, R. A., Dreher, J. W., & Cowan, J. J. 1984, *ApJ*, 285, L35
 Perley, R. A., & Taylor, G. 1991, *ApJ*, in press
 Röser, H.-J., & Meisenheimer, K., eds. 1989, *Radio Hot Spots in Extragalactic Radio Sources* (Heidelberg: Springer-Verlag)
 Salter, C., et al. 1989, *A&A*, 220, 42
 Scheuer, P. A. 1974, *MNRAS*, 166, 513
 ———. 1989, in *Radio Hot Spots in Extragalactic Radio Sources*, ed. K. Meisenheimer & H.-J. Röser (Heidelberg: Springer-Verlag), 159
 Scheuer, P. A., & Williams, P. J. 1968, *ARA&A*, 6, 321
 Siah, M. J., & Wiita, P. J. 1990, *ApJ*, 363, 411
 Spangler, S. R. 1979, *ApJ*, 232, L7
 Spinrad, H., & Stauffer, J. R. 1982, *MNRAS*, 200, 153
 Stephens, P. W. 1987, Ph.D. thesis, Univ. of Manchester
 Wentzel, D. G. 1969, *ApJ*, 157, 545
 ———. 1974, *ARA&A*, 12, 71
 Wiita, P. J., & Gopal-Krishna. 1990, *ApJ*, 353, 476
 Williams, A. G. 1985, Ph.D. thesis, Univ. of Cambridge
 Williams, A. G., & Gull, S. F. 1985, *Nature*, 313, 34
 Winter, A. J., et al. 1980, *MNRAS*, 192, 931
 Wright, M. C., & Birkinshaw, M. 1984, *ApJ*, 281, 135
 Zensus, J. A., & Pearson, T. J. 1990, *Parsec Scale Radio Jets* (Cambridge: Cambridge Univ. Press)